Doctoral Dissertation (Shinshu University)

Dynamic analysis of ultrasonic wave propagation in composite materials and its application for damage evaluation

September 2016

LI RAN

CONTENTS

Abstract

In this work, for giving guidance to the further development of high-precision ultrasonic technology in material characterization and defect detection for composite materials, a series of unique approaches are proposed. By means of time-domain finite element analysis of ultrasonic wave propagation in both of fiber- and particle-reinforced composite materials, the dynamic internal stress distribution which is tightly corresponding to the ultrasonic wave propagation behavior is visualized and analyzed. With consideration of the influences of various factors, such as: material viscoelasticity and anisotropy, internal microstructures and defects, interfacial conditions between constituent phases, incident wave characteristics, each individual wave component and corresponding attenuation component are separately and systematically investigated. On the basis of above studies, the detailed influence mechanisms of aforementioned factors on ultrasonic wave propagation, attenuation characteristics and material viscoelastic properties are clarified.

1) A new method to evaluate dynamic stress distribution of composite materials is proposed by using ultrasonic wave propagation analysis. In the method, a two-dimensional bimaterial composites with elliptical defect is modeled by using the finite element analysis code, “PZflex”. During the ultrasonic wave propagation, the deformation of the composites model and the internal dynamic stress distribution are

visualized and investigated. The influences of material anisotropy on wave propagation are took into consideration, by changing the elastic modulus ratio between fiber and matrix layer, E_f/E_m. Under different anisotropic properties, the influences of stress singularities at defect tips and the free edge of interface, as well as the waveform conversion at interface, on ultrasonic wave propagation and internal stress distribution are evaluated. The simulation results showed that, the method using ultrasonic wave propagation analysis is a convenient and effective way to study the interrelationship among the material properties, internal microstructures and defects, and dynamic internal stress distribution in composite materials.

2) When ultrasonic waves propagate in composite materials, the attenuation characteristics result from the combination effects of various factors, such as material anisotropy and viscoelastic property, internal microstructure and interfacial conditions, incident wave characteristics and so on. Based on the aforementioned method for analyzing the dynamic internal stress distribution, the detailed influence mechanisms of the above factors on ultrasonic wave attenuation characteristics are investigated. In this chapter, a unique approach is proposed, in which each attenuation component can be extracted from the overall attenuation and separately discussed. The variation behaviors of each component against material anisotropy and matrix viscosity are separately and

quantitatively evaluated. From the analysis results, the energy dissipation at fiber/matrix interface is a major component in ultrasonic wave attenuation characteristics, which can provide a maximum contribution rate of 68.2 % to the overall attenuation, and each attenuation component is closely related to the material anisotropy and viscoelasticity.

3) Based on the aforementioned methods, a further study with consideration of the frequency characteristics of each individual attenuation component is carried out. In this chapter, based on the two-layered fiber/matrix composite materials model, by means of extracting the individual attenuation components (viscoelastic attenuation, scattering attenuation due to interfacial defects, and energy dissipation at the interface) from the overall attenuation respectively, the frequency characteristics of each of them with consideration of different material anisotropy and viscoelasticity are quantitatively evaluated. From the results, the ultrasonic wave attenuation during the propagation in layered composite material is mainly due to the matrix viscosity and interfacial interactions, and all attenuation components represent frequency dependence. At low frequencies, energy dissipation at the interface is the main content of the overall attenuation, then the material viscoelastic properties. At high frequency, the effect of the matrix viscosity on the overall attenuation became more significant. Through the present analysis, we can quantitatively evaluate the detailed correlation between the various effect

factors and the individual ultrasonic attenuation components, especially the frequency characteristics.

4) The work in this chapter is dedicated to the practical ultrasonic testing experiment, which is for evaluating the dynamic mechanical characteristics of particle reinforced composite materials. Through a unique material evaluation method, Ultrasonic Dynamic Mechanical Analysis (U-DMA), the dynamic viscoelasticity of particulate composites with different types and contents of particles are measured directly in high frequency domain. In order to clarify the influence mechanisms of distributed particles, on the basis of proposed methods, the ultrasonic wave propagation behaviors due to multi-reflection and scattering waves by particles and matrix viscoelasticity, especially the mutual interactions among particles, are systematically investigated. The individual wave components and attenuation components are also separately and quantitatively discussed. The results clarify that the interactions among particles are playing a major role in ultrasonic wave propagation and attenuation properties, which can significantly affect the viscoelastic characteristics of developed materials. The feasibility and effectiveness of U-DMA and the proposed methods are verified from both simulation and practical experiments.

Chapter 1

General Introduction

Chapter 1: General Introduction

1.1 Ultrasonic Testing Technology

Nondestructive testing (NDT) & nondestructive evaluation (NDE) technologies, since it can allow parts and materials to be inspected and measured without damaging them, have been widely used as a critical method for ensuring the safety and reliability of the parts, structures and systems. Among various kinds of NDT & NDE methods, Ultrasonic Testing Technology, because of its outstanding sensitivity, accuracy and utility come from the high frequency, has been one of the most effective and common used method, and widely applied in various fields [1-6]. Along with the development of signal processing technology and computer science, ultrasonic testing technology has been not only applied for flaw detection but in material characterization, due to the tight connection between ultrasonic propagation characteristics and material physical properties. Accordingly, the extension of application makes the accuracy and reliability of ultrasonic testing technology to be set a higher requirement. For ultrasonic testing in composite materials, because of the lack of further understanding of complex wave propagation behaviors, and the influence mechanism of various factors, such as material anisotropy and viscoelasticity, internal microstructure and interfacial bonding condition, and the

incident wave characteristics, there still have some limitations during the practical application. Therefore, it is of essential importance to establish methods which can systematically investigate the ultrasonic wave propagation behaviors, especially the individual wave components and the corresponding attenuation components, for giving guidance to the further development of high-precision ultrasonic technology in material characterization and defect detection.

1.2 Composite Materials

A composite material is basically a combination of two or more constituent materials for enhancing the stiffness and strength or obtaining the expected characteristics different from the individual components. It can be classified into roughly two types: Fiber reinforced composite materials and Particulate composite materials, which is depending on the type of reinforcement. The internal microstructure and interfacial condition, and physical properties of the constituent phases jointly determine the characteristics and performance of composite materials, and relate closely to the internal stress distribution condition. When external load is applied, due to the presence of geometric and elastic properties discontinuities, concentrated stress field can occur in regions near the interface or around the internal flaw. For instance, in fiber-reinforced composite materials, the

stress singularity can occur at the vicinity of the free edges, which is known as “Free edge effects”; while in particulate composite materials, the concentrated stress fields can be found at the interface between the particle and matrix. These singular behaviors of internal stresses can have marked influences on material performance, and have been observed to be responsible for the initiation and growth of damage, such as delamination or matrix cracking. With the increased utilization of composite materials in various areas, for purpose of prevent early failure and accurate determination of the stress distribution within the composite materials, numerous researches have been carried out, especially for the “Free edge effect” [7-16], interlaminar stress [17-22], and the stress fields in particulate composites [23-25].

1.3 Wave Propagation in Composite Materials

Considering the practical application, the composites structure is always subjected to dynamic loads, which can be discussed from the view point of stress wave propagation. When the stress wave propagates in an isotropic material, from Hooke’s law, the stress-strain relationship for two-dimensional plane strain is written as follows [26]:

$$\sigma = c\varepsilon \tag{1}$$

$$c = \begin{bmatrix} \lambda + 2\mu & \lambda & 0 \\ \lambda & \lambda + 2\mu & 0 \\ 0 & 0 & \mu \end{bmatrix} \tag{2}$$

$$\sigma = [\sigma_{xx} \quad \sigma_{yy} \quad \sigma_{xy}]^T \tag{3}$$

$$\varepsilon = [\varepsilon_{xx} \quad \varepsilon_{yy} \quad \varepsilon_{xy}]^T \tag{4}$$

Where λ and μ are lamé constants, and the T superscript denotes the transposition. Then, the stress wave equations of motion are [27]:

$$\left.\begin{aligned} \frac{\partial \sigma_{xx}}{\partial x} + \frac{\partial \sigma_{xy}}{\partial y} &= \rho \frac{\partial^2 u_x}{\partial t^2} \\ \frac{\partial \sigma_{yy}}{\partial y} + \frac{\partial \sigma_{xy}}{\partial x} &= \rho \frac{\partial^2 u_y}{\partial t^2} \end{aligned}\right\} \tag{5}$$

where, the first term on the left-hand side in Eq.(5) corresponds to a longitudinal wave, and the second term corresponds to a transverse wave. ρ is density. Thus, the corresponding relationship between stress distribution and stress wave propagation can be obtained.

As the dynamic loads are applied, stress waves start to propagate within the composite materials. When the waves propagate along the interface or reach the internal flaw, not only the stress concentration will occur, but the wave propagation characteristics will also be affected, such as the development of shear stress wave and scattering wave, the dispersion of phase velocity and frequency, and the corresponding wave energy dissipation. Accordingly, the wave propagation behaviors can reflect the characteristics of constituent phases and the features of internal microstructure, and even interfacial

condition within the composites. Thus, by investigating the wave propagation behaviors and the corresponding attenuation characteristics, both of the determination of dynamic internal stress distribution and the characterization of material properties of composite materials can be carried out.

1.4 Ultrasonic Testing for Composite Materials

1.4.1 Early Work for Ultrasonic Testing in Composite Materials

Since the advantages of non-destruction and high-efficiency, the ultrasonic testing technology found early applications in defect detection [28]. Initially, measurements of ultrasonic wave attenuation is a commonly employed method for the non-destructive evaluation of polymer-based fiber composites, which is due to the directly correlation between wave attenuation, void content and wave frequency [29]. By using single-frequency C-scans, the attenuation characteristics are also used to detect delaminations, voids and local variations of fiber-resin ratio [30]. Although the independent scattering waves by internal inclusions or defect can be calculated based on the classic scattering theory, since it is difficult to separate the scattering waves during the practical measurement, the detailed mechanism of scattering waves due to internal void or inclusions are not clear. The ultrasonic velocity are also used in the characterization of

the properties of bulk composite materials and detection of interfaces between the different constituent phases. It is found that, the dispersion characteristics of waves were very sensitive to the number of layers and the properties of the interface between bonded layers [31].

It is clear that, the ultrasonic wave propagation can also reflect the viscoelastic properties of composite materials, such as the corresponding relation between phase velocity and elastic modulus, wave attenuation characteristics and loss modulus. Accordingly, the ultrasonic testing are also applied in the characterization of material dynamic mechanical analysis [32], for monitoring the variation of material viscoelasticity as a function of frequency or temperature. From Lionetto's work [33], the ultrasonic dynamic mechanical analysis was proved to be a potential and powerful method for the characterization of polymer, particularly in the manufacture of polymer matrix composites. However, in most of the early works, because of the inherent complexities associated with separately investigating the wave components, there are lack of exact methods or solutions can clarify the influence mechanisms of internal microstructures, such like fibers, distributed particles, and even internal defects, on the material viscoelastic properties.

1.4.2 Investigation of Ultrasonic Wave Propagation in Fiber-reinforced Composite Materials

Due to the difficulty in measurement of the individual wave components from the complex wave signals containing coupled influences of various factors during the actual ultrasonic testing process, numbers of studies have been carried out on the independently investigation of the wave scattering due to internal inclusions, and the corresponding attenuation characteristics, by means of theoretical analysis or numerical simulation. Initially, based on the early theoretical works, the scattering wave propagation in fiber-reinforced composite materials with randomly distributed fibers was carried on. Bose et al. [34] analyzed the time harmonic scattering wave propagation behaviors, with considering of the correlation among phase velocity, attenuation characteristics, statistical and mechanical parameters of the composites. Also by using statistical averaging procedures and a self-consistent multiple scattering theory, Vardadan et al. [35] studied the scattering waves, with consideration of the correlation among the orientation of the scatters, direction of incident waves and the phase velocity, as well as the attenuation characteristics. The studies about the wave scattering behaviors and the attenuation characteristics in void containing fiber reinforced composite materials were also carried out in early years. And it has already know that the ultrasonic attenuation is composed by

the matrix viscosity and the wave energy dissipation due to wave scattering from the internal microstructure and flaws. Williams et al [36] studied the wave attenuation due to the wave scattering by voids in fiber composites. In Hale's work [37], the ultrasonic attenuation due to the spherical voids randomly distributed in fiber-reinforced composite materials was discussed, with consideration of different void ratio and void radius. In the early researches, the theoretical predictions of the scattering waves and attenuation characteristics have been shown to be in good agreement with experimental results at low volume concentrations of the fibers, yet it is difficult to ascertain the influence mechanisms of scattering waves on overall ultrasonic propagation, and the dynamic stress distribution.

Thus, numerical analysis were introduced into the investigation of ultrasonic wave propagation in composite materials, and overcome the limitations of the analytical methods. Based on the Generalized Self Consistent Model (GSCM), Yang [38] studied the multiple scattering effect by fibers, especially for the scattering wave components, such as anti-plane (SH waves) and in-plane (P and SV waves) in fiber-reinforced composite materials with higher concentrations and under higher frequency ranges. For the effect of the fiber-matrix interphase on ultrasonic waves, Huang et al [39] developed a transfer method, in which the dispersion during the wave propagation, and the scattering

waves due to the interactions among multilayered fibers were investigated. In his another work [40], the significantly effects of interfacial condition on the scattering waves was also clarified. For the multi-scattering waves due to internal microstructures in fiber-reinforced composite materials, based on the classic scattering theory, Biwa et al [41-42] studied the independent scattering wave and the corresponding attenuation, and derived the approximate expression of ultrasonic wave components, such as absorption and scattering attenuation component.

In the above methods, the establishment of internal damages and the anisotropic nature for fiber reinforced composite material models are still the limitations. Thus, finite element method, since its versatility to fit the characteristics of each problem, i.e., it allows the use of non-uniform grids and elements with varying characteristics, size and geometry, and even varying the material anisotropy, have been widely used in the ultrasonic propagation analysis for composite materials in recent years [43-46]. Datta et al [47] developed a two-dimensional plane strain finite element model with absorbing boundary condition. By simulating the experimental pulse echo, frequency domain feature analysis in a composite materials with certain types of flaw was done. Mode conversion and scattering due to the flaw were also studied. In Chang' work [48], by means of varying the interface form and the fiber content, the variation behavior of the

transmitted energy ratio, multi-reflection waves and the propagation behaviors were investigated, and the correlation among the ultrasonic waves including reflected waves, transmitted waves and scattering waves, the changed interface form and the distributed fibers were clarified.

1.4.3 Investigation of Ultrasonic Wave Propagation in Particle-reinforced Composite Materials

Unlike the case in fiber-reinforced composite materials, the ultrasonic wave propagation in particle-reinforced composites are mainly affected by the following factors, such as matrix viscoelastic properties, the shape, dimension, content and the distribution of particles and defects, bonding conditions between the constituent phases, and incident wave characteristics. In actual ultrasonic Testing, the measurement of ultrasonic waveforms, phase velocity and attenuation characteristics are the main issue, which are also the important research object in the investigation of ultrasonic wave propagation in particulate composite materials. In early work, Kinra et al [49] studied the phase velocities of longitudinal and shear waves, and attenuation of longitudinal waves, in an actual experiment for random particulate composites with low concentration of particles. From his work, the validity of several theoretical predictions for assessing the attenuation in

particulate composites were confirmed. For the scattering effect and viscoelastic losses in a random particulate viscoelastic composites, Beltzer et al [50] established a new method including the computation of the scattering losses and the viscoelastic losses, as well as the subsequent application of the Kramers-Kronig relationships to derive the wave speed. In the method, the matrix was considered as a viscoelastic media with linear law of attenuation. In Datta's work [51], a unique model of particulate composite materials was established, in which the random distributed spherical particles were separated from the matrix by thin layers of elastic material. Then, the wave propagation was carried out, and the attenuation and phase velocity for both longitudinal and shear waves were investigated. At this time, the independent scattering waves from individual particles cannot still be evaluated.

Then, based on the classic scattering theory, Biwa et al [52–54] established a theoretical model for particulate viscoelastic composite materials for investigating the independent scattering attenuation due to particles and the absorption attenuation due to the matrix viscous nature. In his model, the independent scattering by particles was directly related to not only the particle content, but also the scattering cross-section of the individual particle, which was related to the physical properties of the constituent phases and the incident wave frequency. Mylavarapu et al [55] also developed a model for

computing ultrasonic attenuation coefficient in particulate composites, with consideration of the effects of radius ratio, particle size, and the porosity on attenuation. However, in all of the above investigations, the interactions between particles which is tightly connected to the multi-scattering waves are neglected.

1.5 Outline of the Dissertation

From the previous works, it is clear that, the dynamic internal stress redistribution, the individual wave components and the corresponding wave attenuation characteristics are the core issues to obtain further understanding of ultrasonic wave propagation within the composite materials. So far, there is still no well-defined method or solution which can systemically and detailedly investigate each individual ultrasonic wave component and the corresponding attenuation components with considering the influences of various factors, such as the internal microstructures and defects, material anisotropy and viscoelastic properties, and the interfacial condition between constituent phases.

Therefore, in the present dissertation, on the basis of newly developed finite element code for ultrasonic wave propagation analysis, “Pzflex”, the complex ultrasonic wave propagation behaviors within fiber- or particle-reinforced composite materials with interfacial defect can be visualized and well investigated. Herein, the detailed influences

of internal stress singular behaviors, viscoelastic and anisotropic properties of constituent phases, and incident wave characteristics on wave propagation, attenuation and viscoelastic characteristics are emphasized and detailedly studied. And based on the results from the present methods, we can provide guidance to the further development of ultrasonic testing technology for damage detection and material characterization. In this dissertation, the detailed contents are as follows:

Chapter 1 General Introduction

The application of ultrasonic testing in composite materials was introduced. A brief summary for correlation researches about ultrasonic wave propagation in Fiber-reinforced composites and particulate composites are presented.

Chapter 2 Dynamic Stress Analysis in Bimaterial Composite with Defect Using Ultrasonic Wave Propagation

A two layered bimaterial composite model with a transverse elliptical defect is analyzed under a time-harmonic longitudinal incident wave, and the complicated ultrasonic wave propagation at each layer are simulated. Based on the direct correspondence between waveform and internal stress fields in the material, the dynamic internal stress distribution is visualized and analyzed. The characterization of internal

dynamic stress distribution varying with material properties, and the influence of stress concentration at defect tips and the free edge of interface on the ultrasonic propagation are clarified.

Chapter 3 Quantitative Evaluation of Ultrasonic Wave Attenuation Components in Bimaterial Composites with Defect

On the base of ultrasonic wave propagation analysis in the 2-D two layered composite materials aforementioned in chapter 2, all individual attenuation components are extracted from the overall attenuation and detailedly evaluated, with consideration of the influence of material anisotropy and matrix viscosity..

Chapter 4 Analysis of Individual Attenuation Components of Ultrasonic Waves Considering Frequency Dependence

Based on the aforementioned method which can separately and quantitatively investigate the attenuation characteristics, the frequency characteristics of each attenuation component are separately discussed with consideration of different material viscosity and anisotropy.

Chapter 5 U-DMA Measurement and Dynamic Analysis of Ultrasonic Wave Propagation in Particulate Composites

Ultrasonic Dynamic mechanical analysis (U-DMA), as a new ultrasonic testing technology for material characterization, has been applied to the viscoelasticity evaluation of particle reinforced polymer composites with different type and content of particles. In order to systematically investigate the influence mechanism of particles, by means of the method in previous chapter, which can separately evaluate the wave component and corresponding attenuation components, the multi-reflection and scattering waves due to particles, and the corresponding attenuation components, are emphasized and discussed with consideration of the mutual interactions among particles.

Chapter 6 General Conclusion

General conclusions about the present dissertation are presented.

References

1. Ultrasonic technique handbook, Nikkan Kougyou Shinbunsya, (1960), 1352 [in Japanese].

2. H. Yamawaki, Non-Destruct. Inspect., 47 (1998) 243 [in Japanese].

3. F.D. Hastings, J.D. Schneider, S.L. Broschat, J. Acoust. Soc. Am., 100 (1996) 3061.

4. Y. Cho, J.L. Rose, J. Acoust. Soc. Am., 99 (1996) 2097.

5. G. Wojcik, J.A. Mould, L.S. Carcione, *Proc. IEEE* Ultrason. Symp., (1998) p.1.

6. G. Wojcik, B. Fornberg, R. Waag, L. Carcione, J. Mould, L. Nikodym, T. Driscoll, *Proc. IEEE* Ultrason. Symp., (1997) p.1501.

7. N.J. Pagano, Int. J. Solids Struct., 14 (1978) 401.

8. I.S. Raju, J.H. Crews, Comput. Struct., 14 (1981) 21.

9. J.D. Whitcomb, I.S. Raju, J.G. Goree, Comput. Struct., 15 (1982) 23

10. W.H. Chen, T.F. Huang, Compos. Struct., 32 (1989) 1275.

11. L.B. Lessard, A.S. Schmidt, M.M. Shokrieh, Int. J. Solids Struct., 33 (1996) 2243.

12. N.W. klingbeil, J.L. Beuth, Eng. Fract. Mech., 66 (2000) 93.

13. M.H. Cho, H.S. Kim, Int. J. Solids Struct., 37 (2000) 435.

14. M. Tahani, A. Nosier, Compos. Struct., 60 (2003) 91.

15. L. Lagunegrand, T. Lorriot, R. harry, H. Wargnier, J.M. Quenisset, Compos. Sci.

Technol., 66 (2006) 1315.

16. R. Esquej, L. Castejon. M. Lizaranzu, M. Carrera, A. Miravete, R. Miralbes, Compos. Struct., 98 (2013) 121.
17. N.J. Pagano, J. Compos. Mater., 8 (1974) 65.
18. N.J. Pagano, Int. J. Solids Struct., 14 (1978) 385.
19. J.K. Chen, C.T. Sun, Compos. Struct., 8 (1987) 271.
20. C.A. Rose, C.T. Herakovich, Compos. Eng., 3 (1993) 271.
21. A. Nosier, A. Bahrami, Compos. Mater., 78 (2007) 18.
22. A. Andakhshideh, M. Tahani, Composites Part B, 47 (2013) 58.
23. Z.R. Wang, T.K. Chen, D.J. Lioyd, Metall. Trans., 24 (1993) 197.
24. Y.L. Wu, Z.F. Dong, Mater. Sci. Eng., 203 (1995) 314.
25. R. Paskaramoorthy, S.A. Meguid, Compos. Sci. Technol., 59 (1999) 1361.
26. J.L. Rose. Cambridge University Press, London, (1999) 24.
27. J.J. Chang, Q.Q. Ni, M. Iwamoto, Jpn. J. Appl. Phys., 43 (2004) 2926.
28. W. Sachse, B. Castagnede, I. Grabec, K.Y. Kim, R.L. Weaver, Ultrasonics, 28 (1990) 97.
29. D.E.W. Stone, B.Clarke, Non-Destr. Test., 8 (1975) 137.
30. W.N. Reynold, L.P. Scudder, H Pressman, Polym. Test., 6 (1986) 325.
31. S.K. Datta, J.D. Achenbach, Y.S. Rajapakse, *Proc*. *IUTAM* Elast. Wave Propag.

Ultrason. Eval., University of Colorado, USA, (1989).

32. V. Kostopoulos, D.Th. Korontzis, Compos. Sci. Technol., 63 (2003) 1441.

33. F. Lionetto, A. Maffezzoli, Adv. Polym. Tech., 27 (2008) 63.

34. S.K. Bose, A.K. Mal, Int. J. Solids Struct., 9 (1973) 1075.

35. V.K. Varadan, V.V. Varadan, Wave Motion, 1 (1979) 53.

36. J.H. Williams, Jr., S.S. Lee, H. Yuce, NASA Contractor Report, 3693 (1983).

37. J.M. Hale, J.N. Ashton, NDT Int., 21 (1988) 321.

38. R.B. Yang, A.K. Mal, J. Mech. Phys. Solids, 42 (1994) 1945.

39. W. Huang, S. Brisuda, S.I. Rokhlin, J. Acoust. Soc. Am., 97 (1995) 807.

40. W. Huang, S.I. Rokhlin, Y.J. Wang, Ultrasonics, 33 (1995) 365.

41. S. Biwa, T. Shibata, Compos. Sci. Technol. 60 (2000) 83.

42. S. Biwa, S. Yamamoto, F.Kobayashi, N. Ohno, Int. J. Solids Struct., 41 (2004) 435.

43. L.W. Cai, J.H. Williams Jr., Ultrasonics, 37 (1999) 463.

44. M.V. Menshykova, O.V. Menshykov, V.A. Mikucka, I.A. Guz, Compos. Sci. Technol. 72 (2012) 1057.

45. J. Zhang, W.J. Ye, T.X. Yu, Ultrasonics, 53 (2013) 1200.

46. H. yamawaki, T. Saito, NDT&E Int., 33 (2000) 489.

47. D. Datta, N.N. Kishore, NDT&E Int., 29 (1996) 213.

48. J.J. Chang, C.L. Zheng, Q.Q. Ni, Compos. Struct., 75 (2006) 451.

49. V.K. Kinra, M.S. Petraitis, S.K. Datta, Int. J. Solids Struct., 16 (1980) 301.

50. A.I. Beltzer, C.W. Bert, A.G. Striz, Int. J. Solids Struct., 19 (1983) 785.

51. S.K. Datta, H.M. Ledbetter, Y. Shindo, A.H. Shah, Wave Motion, 10 (1988) 171.

52. S. Biwa, Mech. Mater., 33 (2001) 635.

53. S. Biwa, Y. Watanabe, S. Motogi, N. Ohno, Ultrasonics, 43 (2004) 5.

54. S. Biwa, S. Idekoba, N. Ohno, Mech. Mater., 34 (2002) 671.

55. P. Mylavarapu, E. Woldesenbet, Composites Part B, 41 (2010) 42.

Chapter 2

Dynamic Stress Analysis in Bimaterial Composite with Defect using Ultrasonic Wave Propagation

Chapter 2: Dynamic Stress Analysis in Bimaterial Composite with Defect using Ultrasonic Wave Propagation

2.1 Introduction

Composite materials, such as carbon fiber or glass fiber reinforced plastics (FRP), have been applied practically in various fields, such as aircraft, space and other structural fields, owing to their excellent characteristics of light-weight, high rigidity ratio and so on. As the application of composite materials in load-bearing structure increases, it is considerably important to understand the characteristics of dynamic stress distribution and the influence of stress singularities when the composite materials are under dynamic loading. Due to the free edge, interface and the presence of defects, the applied dynamic loading may cause complicated stress distribution and difficult to characterize the interactions between them. Thus, no well-defined method for characterization of dynamic stress distribution in composite materials has been proposed. Since the ultrasonic wave propagation is based on elastic wave theory it should be corresponding to the dynamic stress fields. The wave intensity, amplitude and other characteristics may vary with the material properties, interface behavior and defect shape/size, so that the characterization of wave propagation can be used to study the dynamic variation of internal stress fields in composite materials.

Many investigators have studied the characteristics of ultrasonic wave propagation in composites experimentally and theoretically. Saches [1] reviewed the relative development of quantitative ultrasonic measurements and presented examples of applications of these methods. Rokhlin [2] discussed two potential ultrasonic techniques for characterization of fiber-matrix composites, confirmed that the elastic properties can significantly affect the ultrasonic propagation. By using finite element method, Datta [3] proposed a two dimensional plane strain finite element model to deal with the mode conversion and scattering due to the presence of flaws. By using a computational procedure for multiple wave scattering, Biwa [4] dealt with the ultrasonic propagation and the quantization of attenuation.

The above methods have been applied to investigate the stress wave propagation behavior of ultrasonic waves, especially for the evaluation of scattering wave and wave attenuation. However, for two-layered composite with transverse defect/damage at the fiber/matrix interface, there is no well-defined method for evaluating the complicated scattered wave fields caused by the interactions between layers, and the correlation between the internal stress redistribution and the material properties.

In this chapter, based on time-domain finite element analysis of ultrasonic wave propagation, a new method is developed. A two layered bimaterial composite model with

a transverse elliptical defect is analyzed under a time-harmonic longitudinal incident wave, and the complicated ultrasonic wave propagation at each layer are simulated. Based on the direct correspondence between waveform and internal stress fields in the material, the dynamic internal stress distribution is visualized and analyzed. The characterization of internal dynamic stress distribution varying with material properties, and the influence of stress concentration at free edge and interface on the ultrasonic propagation are clarified. The results of stress concentration factors at defect tips in different material regions also indicate the validity of the present analysis. Through the above, the correlation between internal stress fields and ultrasonic wave characterization is clarified, and the effectiveness of ultrasonic wave propagation as a novel dynamic stress analysis is confirmed.

2.2 Ultrasonic Wave Equations of Motion

On the basis of the ultrasonic wave equations for two-dimensional plane strain in isotropic media as described in section 1.3, the first term on the left-hand side corresponds to a longitudinal wave, and the second term corresponds to a transverse wave. For each of the wave fields, the displacement is given in terms of two potentials ϕ and ψ via the Helmholtz decomposition.

$$u_x = \frac{\partial \Phi}{\partial x} + \frac{\partial \Psi}{\partial y} \qquad u_y = -\frac{\partial \psi}{\partial x} + \frac{\partial \phi}{\partial y} \tag{1}$$

From Hooke's Law, the $\sigma_{xx}, \sigma_{yy}, \sigma_{xy}$ can be rewrite as:

$$\frac{\sigma_{xx}}{2G} = -\frac{\partial^2 \Phi}{\partial y^2} + \frac{1}{2}\kappa^2 \left\langle \frac{\partial^2 \Phi}{\partial x^2} + \frac{\partial^2 \Phi}{\partial y^2} \right\rangle + \frac{\partial^2 \psi}{\partial x \partial y} \tag{2}$$

$$\frac{\sigma_{yy}}{2G} = -\frac{\partial^2 \Phi}{\partial x^2} + \frac{1}{2}\kappa^2 \left\langle \frac{\partial^2 \Phi}{\partial x^2} + \frac{\partial^2 \Phi}{\partial y^2} \right\rangle - \frac{\partial^2 \psi}{\partial x \partial y} \tag{3}$$

$$\frac{\sigma_{xy}}{2G} = \frac{\partial^2 \Phi}{\partial x \partial y} - \frac{\partial^2 \psi}{\partial x^2} + \frac{1}{2}\left\langle \frac{\partial^2 \psi}{\partial x^2} + \frac{\partial^2 \psi}{\partial y^2} \right\rangle \tag{4}$$

Where $k^2 = \frac{2(1-\nu)}{(1-2\nu)}$.

By means of the displacement potentials, the wave equation can be rewrite as:

$$\begin{cases} \frac{\partial^2 \Phi}{\partial x^2} + \frac{\partial^2 \Phi}{\partial y^2} = \frac{1}{C_L^2}\frac{\partial^2 \Phi}{\partial t^2} \\ \frac{\partial^2 \Psi}{\partial x^2} + \frac{\partial^2 \psi}{\partial y^2} = \frac{1}{C_T^2}\frac{\partial^2 \psi}{\partial t^2} \end{cases} \tag{5}$$

$$C_L^2 = \frac{2(1-\nu)G}{(1-2\nu)\rho} \quad , \quad C_T^2 = \frac{G}{\rho} \tag{6}$$

Where C_L and C_T is the longitudinal wave velocity and shear wave velocity. We have got the general expression of displacement field and the stress field. For the presented two-layer material, by adding the boundary condition at edges and fiber/matrix interface, we can calculate the stress fields at each layer. In order to simplify the ultrasonic wave propagation, absorbing boundary condition is assumed on the right side where no reflection wave will occurs, and the upper and lower edges are set to be roller supports. Then, it is clear that, at the upper and lower edges, the shear stress, $\sigma_{xy} = 0$. For the perfect bonded interfacial condition, the displacement and the normal strain in the direction of incident ultrasonic waves at fiber/matrix interface are continuous. And for

the plane longitudinal wave loads along the interface, due to the different material elastic properties, the shear stress waves are all generated from the interlaminar shear between fiber and matrix layers.

When ultrasonic wave impinges on the transverse defect, the internal wave fields can be given by the sum of the incident wave and the scattered waves. The time-harmonic displacement components are

$$u = u^{INC} + u^{SCA} \tag{7}$$

Where the superscript *INC* and *SCA* denote the incident and scattered waves, respectively. By calculating the Time of Flight of waves, we can separate the incident waves and the scattered waves.

2.3 FEM Model

Herein, the Fiber Reinforced Epoxy composite is took into account, which is considered as a double-layer geometric construction. Thus, a simplified two-dimensional bimaterial model with an elliptical defect perpendicularly across the interface is established, just as depicted in Fig.2-1, for different material components with a defect. The coordinates are placed at the free edge of the interface [5-6], where the point A is the origin of the coordinates and the x-axis is along the interface. The upper and lower regions are for fiber and matrix respectively, and they are perfectly bonded at the interface along

$y=0$. The defect lies symmetrically across the interface in the center of model. The following geometric sizes are selected: $L=2h=10\lambda$ (λ,minimum wavelength of incident wave), $a=2b=2\lambda$.The input data of material properties for the analysis are shown in Table 1-1[7].

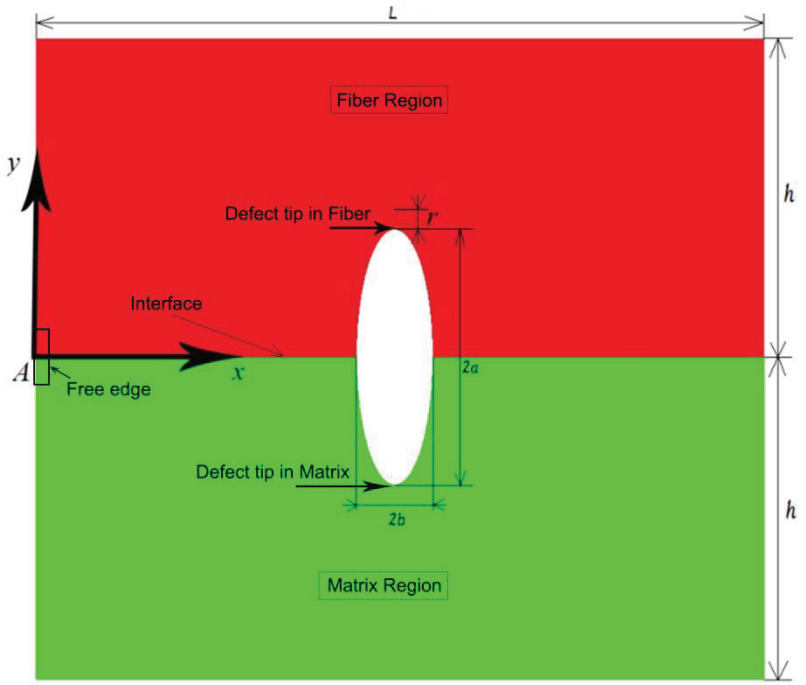

Fig.2-1 Model of bimaterial composite with a defect.

Table 2-1 Material parameters used for analysis.

Materials	Fiber	Resin	Defect
Density (kg/m^3)	2400	1200	0
Longitudinal Velocity (m/s)	6000	3000	0
Transverse Velocity (m/s)	3500	1850	0
Loss (db/m)	0	0	0

In order to simplify the ultrasonic wave propagation, absorbing boundary condition

is assumed on the right side where no reflection wave will occurs, and the upper and lower edges are set to be roller supports. A one-cycle sinusoidal longitudinal wave is vertically applied at the left side, which is assumed to be of amplitude of 1 MPa at the frequency of 1 MHz.

The procedure is shown in the flowchart of the analysis in Fig.2-2. For the specified E_f/E_m, the ultrasonic propagation and internal stress distribution are simulated and analyzed.

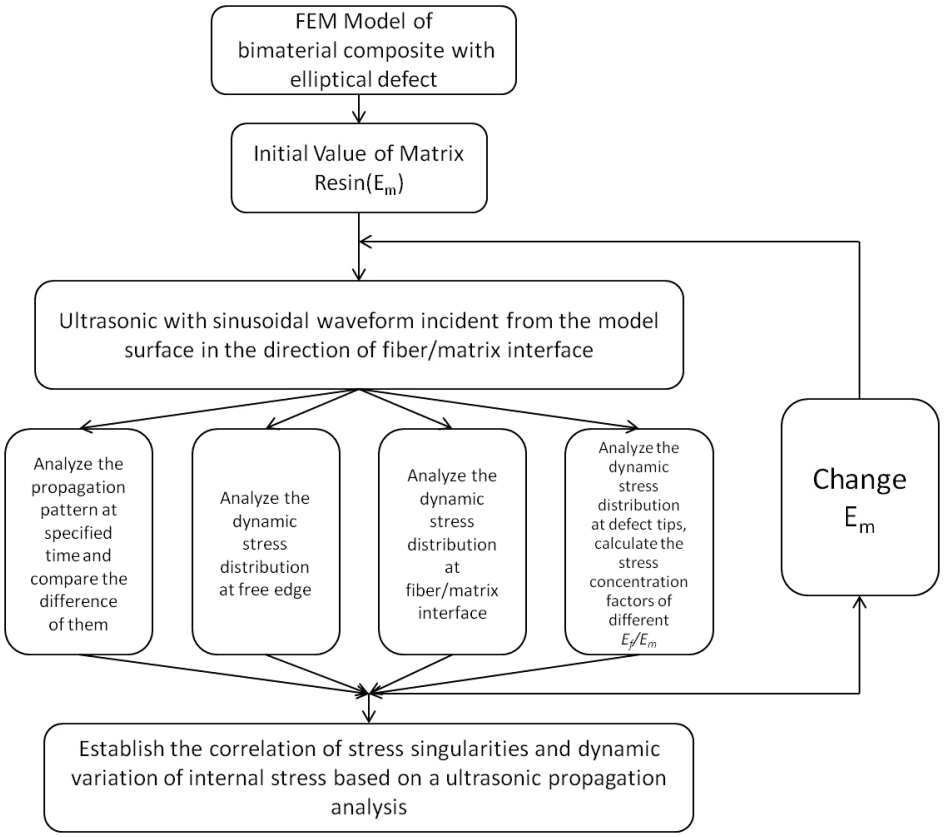

Fig.2-2 Flowchart of the ultrasonic wave propagation analysis.

2.4 Results and Discussion

2.4.1 Ultrasonic Wave Propagation

When ultrasonic wave propagates in a composite material, the stress wave propagation behaviors will depend on material properties. Thus, in order to evaluate the correlation between them, from Eq.(5) in section 1.3, the density is set to different values to make the wave propagation and internal stress distribution changing. Here, five different ratios of E_f/E_m, fiber/matrix= 1, 4/3, 2, 4, 8, are assigned by changing density of matrix (the wave propagation velocity of fiber and matrix are held constant) in order to investigate the influence of the anisotropic property on dynamic stress distribution in the model, where E_f, E_m are the Young's modulus of fiber and matrix, respectively.

The normal stress and shear stress distributions at different times are investigated and then visualized to understand the stress concentration phenomenon at free edge, interface and defect tips. By comparing with the propagation pattern in the models with different E_f/E_m, the influence mechanism of free edge effect and interface stress concentration on the internal ultrasonic wave propagation is investigated.

Fig.2-3 shows the normal stress distribution patterns at different propagation times and different ratios of E_f/E_m. The minimum and maximum stress scale of the color is shown in the bottom of each figure, such as 0-2.08 for E_f/E_m=8. When E_f/E_m = 8 at 0.25ms

(incident wave amplitude at the free edge is just 1MPa), the dark blue region which represents the stress concentration region can be observed at the interface near the free edge, in which the normal stress is 2.08 MPa. The light-color at the left edge is corresponding to the initial incident wave of 1 MPa, while the red part where the incident wave has not arrived is zero. When E_f/E_m decreased from 8 to 1, the concentrated stress at the interface near the free edge decrease and almost disappeared at E_f/E_m=1.

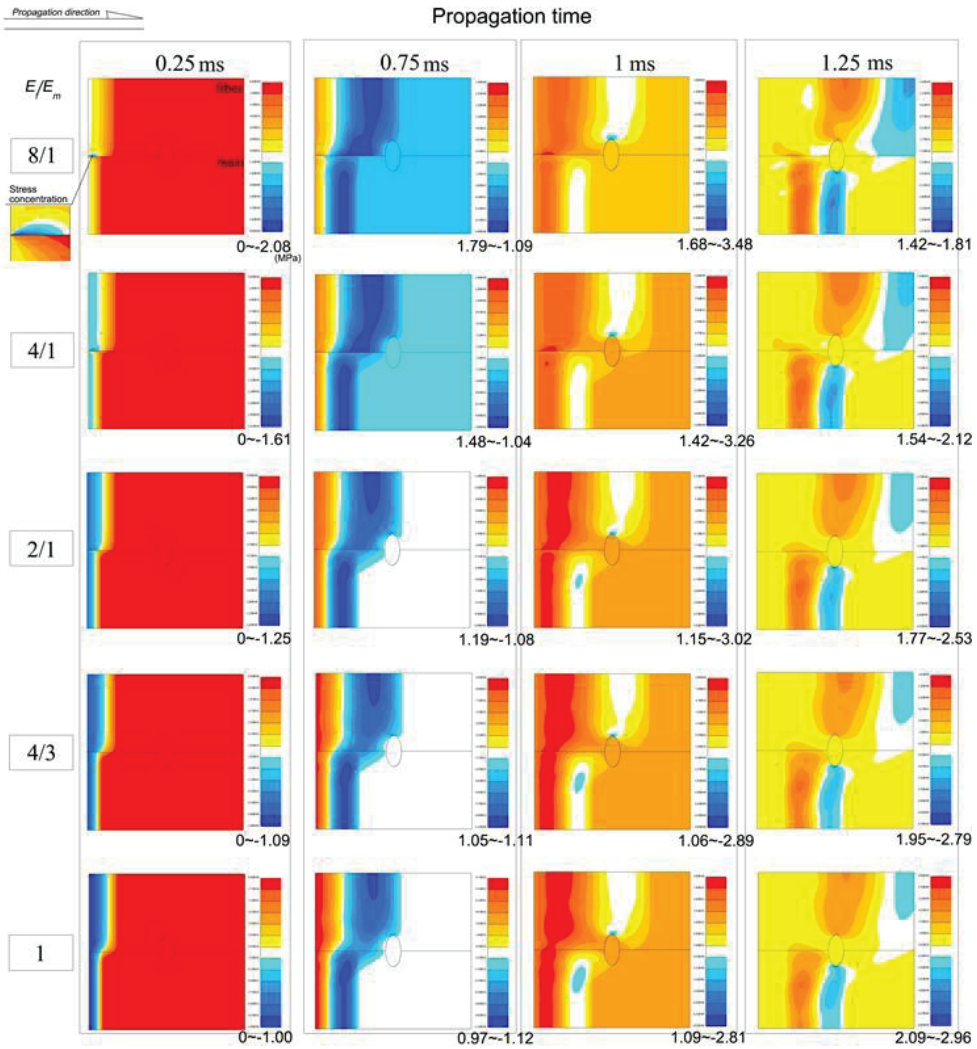

Fig.2-3 Normal stress distribution of different E_f/E_m.

When the incident wave propagated furthermore to the interface, for E_f/E_m =1, the stress distribution at the interface between fiber and matrix regions is continuous, while for E_f/E_m= 8, it is discontinuous. From the stress pattern changing at free edge and interface, it is clear that the stress concentration and stress redistribution during the wave propagation depend significantly on the material anisotropic properties.

When the wave fronts reached the defect tips in fiber and matrix region respectively, at t=1 ms and 1.25 ms, since the ultrasonic wave propagation has been affected by the scattering wave from free edge and interface, the wave patterns at the defect tip become more complicated and the stress concentration factor at defect tip in fiber region and matrix region become different, which is obviously different from that of isotropic material. For example, at E_f/E_m=8, the difference of the maximum stress at defect tips of fiber and matrix region is 1.14 MPa, while at E_f/E_m=1, it is about 0.15 MPa.

In order to discuss the wave propagation at the interface near the free edge, the enlarged stress distribution patterns for different E_f/E_m are illustrated in Fig.2-4. The angle α represents wave propagation direction, where α=0 for the initial incidence wave. Since the interface was assigned to be perfectly bonded, the different strains of fiber and matrix region led to the interface bending, and this made the wave propagation direction changed. When E_f/E_m =1, the stress distribution at interface is successive due to the same elastic

modulus. But because of the relatively small density of fiber region, the deformation of fiber region becomes bigger than that in matrix region and this resulted in the wave propagation angle to be the minus value, indicating propagation from fiber region to matrix region.

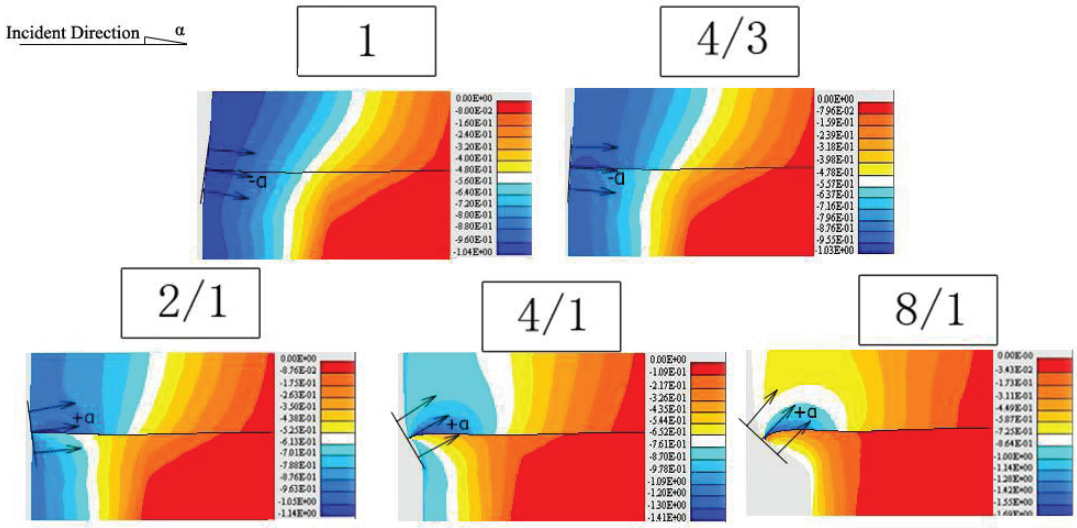

Fig.2-4 Ultrasonic wave propagation direction of different E_f/E_m.

With E_f/E_m increasing, the propagation angle α changes from -α to +α , that means the ultrasonic wave propagates from the mode of "fiber to matrix" to "matrix to fiber". From the above, it is clear that the material properties closely related to the propagation of ultrasonic wave, and by changing the E_f/E_m, the ultrasonic wave pattern, namely, the internal stress distribution can be controlled.

2.4.2 Dynamic Stress Distribution

2.4.2.1 Stress Distribution at Free Edge

At first, the free edge effect in the bimaterial composite is discussed. The free edge effect is mainly explained by the material discontinuity between two layers, which is characterized by the concentrated stress fields at the free edges. For composite materials combining different components together, the free-edge effect is an important issue in the prediction of mechanical property. Various approaches have been used to predict the free edge effects of composite laminates under in-plane loading. The oldest numerical method approaches in this field used finite differences by Pagano [8-9] he proposed an approximate theory based on an extension of Ressner's variational principle to laminated body. Here, we tried to use time domain FEM analysis of wave propagation to discuss the stress variation at the free edge interface of bimaterial composite to clarify the dynamic stress distribution during the wave propagation.

The free edge effect at the free edge of fiber/matrix interface is characterized by the maximum value of dynamic stresses when the ultrasonic wave loads are applied. As shown in Fig.2-5 (a), *x* in the fiber region increased from 1 MPa to the peak value, which is more than twice of the normal incident wave when E_f/E_m=8, while x in the matrix region is in opposite variation to that in fiber region. When the E_f/E_m increased from 1 to 8, the maximum value of normal stress in x direction increased obviously in fiber region, while it decreased to less than half of the incident wave in matrix region. The calculated normal

stress ratio of the maximum value to incident load at the free edge in fiber region and matrix region is presented in Table 2-2 for comparison.

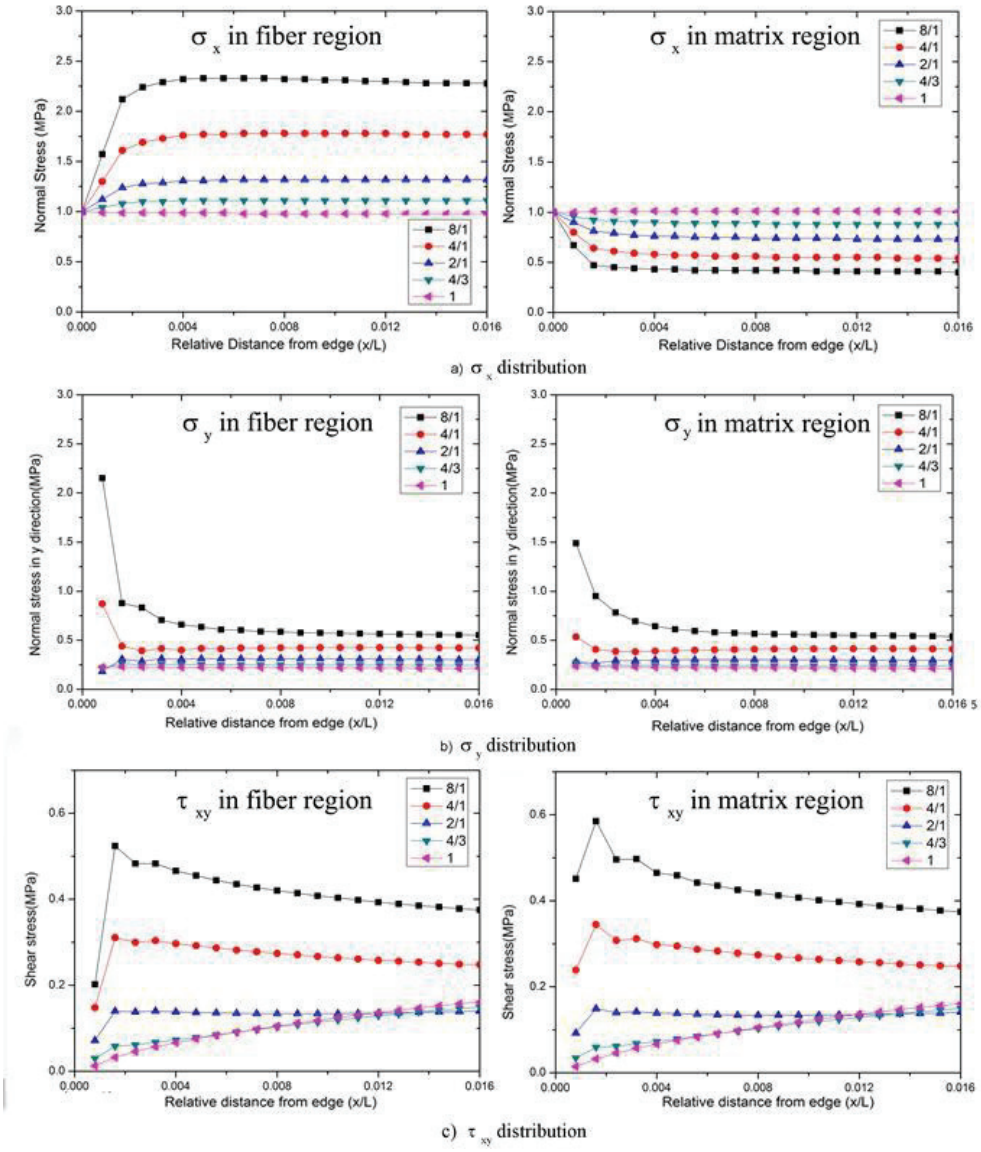

Fig.2-5 Stress distribution at free edge of different E_f/E_m.

Table 2-2 Normal stress ratio at defect tip for different E_f/E_m.

		Modulus ratio				
		8	4	2	4/3	1
Normal stress ratio	Free edge in Fiber	2.33	1.77	1.32	1.11	0.99
	Free edge in Matrix	0.41	0.55	0.76	0.90	1.00

Fig.2-5(b) shows the y direction normal stress distribution with the different E_f/E_m. When E_f/E_m =8, a significant peak appears at the vicinity of free edge, with its value of 2.23 MPa in fiber region and 1.49 MPa in matrix region. This stress singularity can be considered as the peeling stress at interface due to free edge effect, which is caused by the strain difference in fiber and matrix region for a perfect bonding interface. With the increasing of relative distance from the edge (x/L) during the wave propagation, due to the interlaminar shear, the drop dramatically to be stable at 0.55 MPa.

When E_f/E_m=4, the maximum at free edge decreased, with its value of 0.83 MPa in fiber region and 0.55 MPa in matrix region, then stabilized at 0.4 MPa. With the E_f/E_m decreased to 1, since the interface bending become smaller as shown in Fig.2-4, no stress singularity can be seen at free edge, and the decreased to 0.25 MPa.

Fig.2-5(c) shows the variation of τ_{xy} at different E_f/E_m. The interlaminar shear stress, τ_{xy}, at E_f/E_m=1 is 0.06 MPa, while it reached the peak value of 0.53 MPa at E_f/E_m=8. With

the increasing of E_f/E_m, the interlaminar shear stress becomes smaller as depicted in Fig.2-4 due to the strain difference in fiber layer and matrix layer.

2.4.2.2 Stress Distribution at Interface

When ultrasonic wave propagates beyond the free edge region, the stress distribution at the interface is affected not only by the free edge effect but also by the material anisotropy and the internal defects.

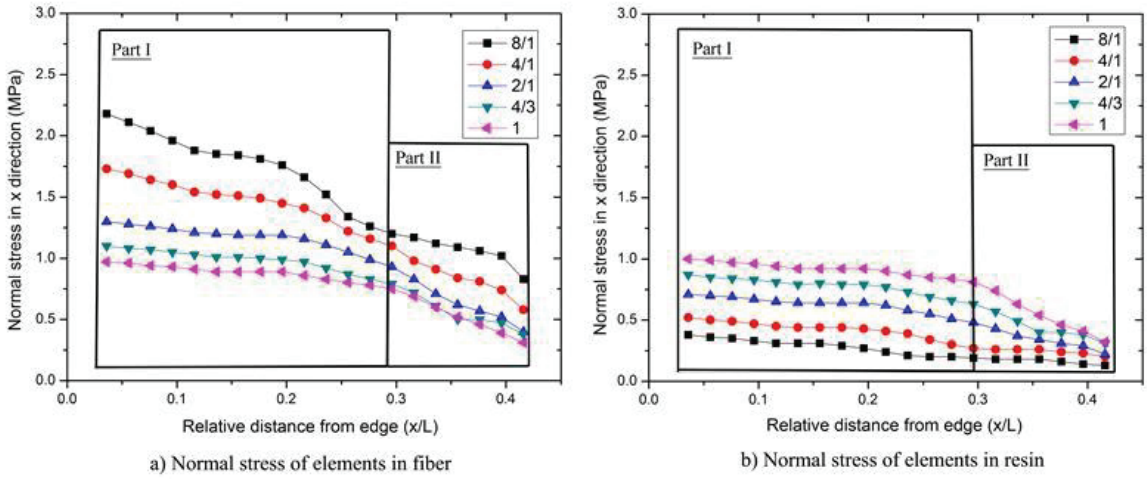

Fig.2-6 Stress distribution at the fiber/matrix interface with different E_f/E_m.

Fig.2-6 shows the normal stress and shear stress distribution at the positions of relative distance x/L=0.03 to 0.4 (close to the defect). From the normal stress distribution, the variation curves of normal stress at the interface during the positions of x/L=0.03 to 0.4 can be departed into two parts (see Fig.2-6). In part I, the stress concentration is mainly contributed by free edge effect and the mode conversion of stress occurs at

interface due to the interlaminar shear. For the part II, the low stress value is as a result of the stress redistribution due to the presence of defect. The decrease of normal stress can be observed in both fiber and matrix regions as depicted in Fig.2-6(a) and (b). For E_f/E_m=8 with the change of the positions of relative distance from x/L=0.03 to 0.4, the normal stress in fiber region decreased from 2.2 MPa to 0.8 MPa, while in matrix region it decreased from 0.4 MPa to 0.1 MPa. With the E_f/E_m decreasing to 1, the normal stress at the interface becomes similar in both fiber region and matrix region, no obvious difference is observed.

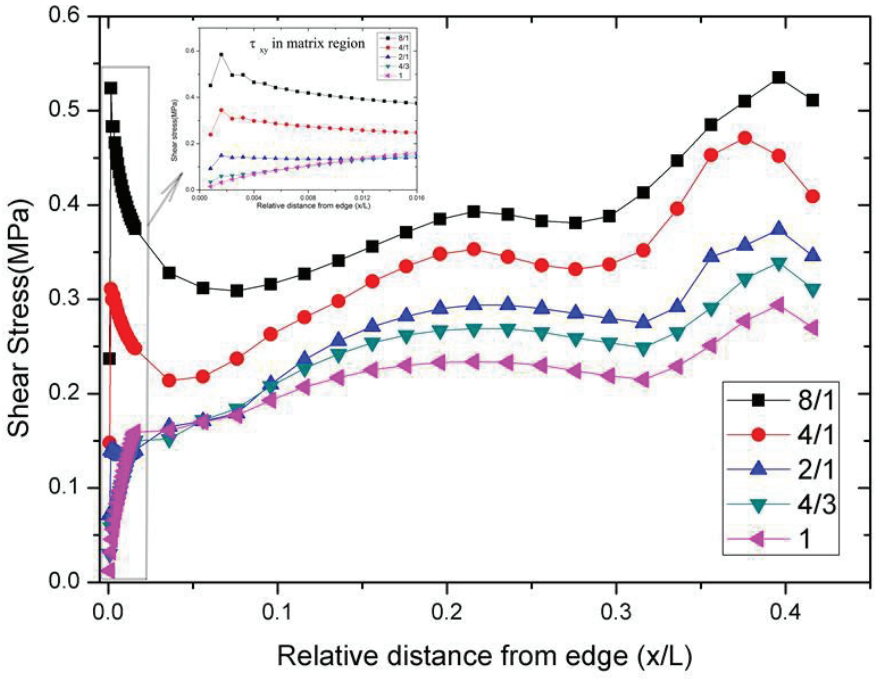

Fig.2-7 Shear stress distribution at the fiber/matrix interface with different E_f/E_m.

The shear stress distribution from free edge (x/L=0) to the defect (x/L=0.42) is shown

in Fig.2-7. For E_f/E_m=1 and 4/3, the shear stress increased from the free edge since the normal strain difference in fiber region and matrix region increased with the ultrasonic wave propagation, but no singularity of shear stress at the free edge is observed. For large E_f/E_m, such as 8, the singularity at the free edge becomes obvious and the maximum value of shear stress is about 0.58 MPa at the free edge is confirmed. During the propagation, the shear stress value shows a tendency that, decreases at $0<x/L<0.05$, then rises till the waves reach the position at x/L=0.4, and slightly drop at x/L=0.42. It is clear this singularity and the local shear stress variation depend greatly on the values of E_f/E_m.

The dynamic stress distribution at interface can be considered as a result of the superposition of waves in fiber region and matrix region. From the waveform during the propagation, we can know how waves from fiber region and matrix region superposed to result in the presented stress distribution.

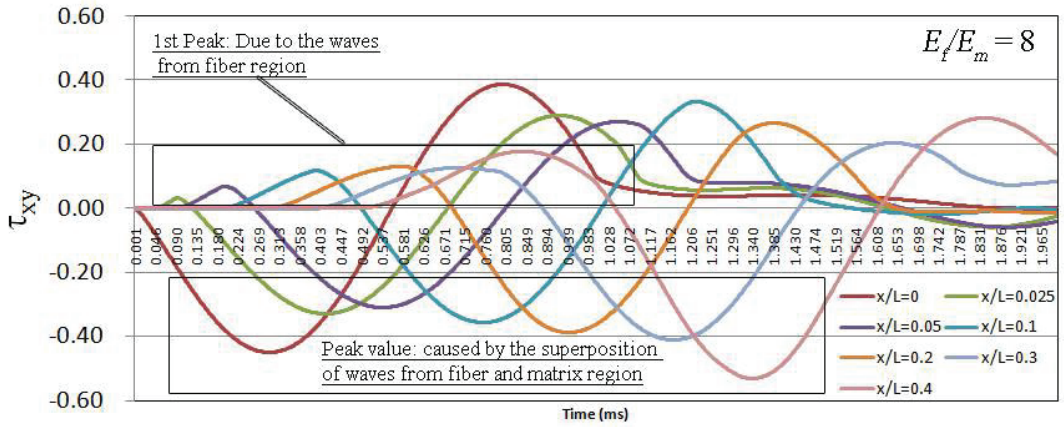

Fig.2-8 Stress waveform at different distance from the free edge with E_f/E_m=8.

Fig.2-8 shows the shear stress waveform of E_f/E_m=8 during the propagation. When the ultrasonic wave started to propagate into the free edge, the normal strain in matrix region is much larger than that in fiber region, and this resulted in the occurrence of the shear stress waveform at the free edge interface area. With the x/L increasing, since the different propagation speed, the elements at interface subject to the ultrasonic waves from fiber region and matrix region successively, which leads to the waveforms of x/L>0 as depicted in Fig.2-8.

Here, the peak values (negative phase) of the superposed shear stress waveform at the different positions are used for comparison. At x/L<0.05, due to the time difference of arrival of the two waves from fiber and matrix region is small, the result of wave superposition shows destructive interference, which results in the decrease of peak value. When the relative distance increased from x/L=0.1 to 0.4, with the increasing of the distance between the two wave fronts in fiber and matrix region, the peak value of shear stress wave become larger. During x/L=0.4 to 0.42, the shear stress value slightly reduced, which is also affected by the boundary conditions of the zone near the defect and the reduction may be mainly due to the free boundary of the defect.

In order to know how interface stress influence on wave propagation, the reflection echo in the elements of the free edge was investigated. Figure 2-9 shows the waveform

of x at free edge with different material properties. The first cycles are corresponding to the incident waves, and the normal stresses occurred with the same cyclic period but varied amplitudes are corresponding to each value of E_f/E_m.

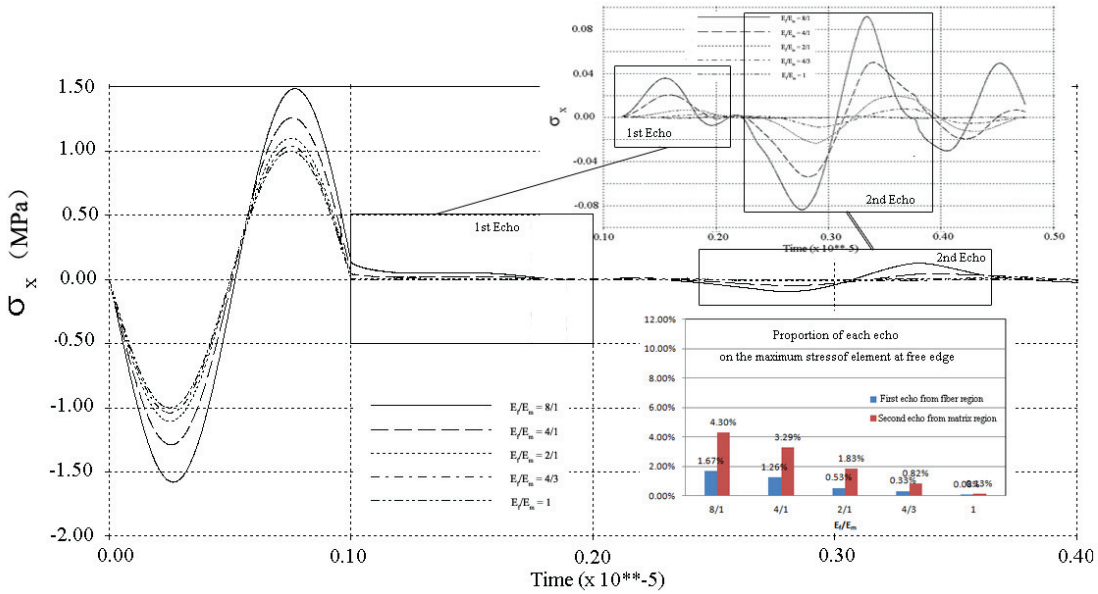

a) Variation of normal stress of element at free edge in fiber region with different E_f/E_m

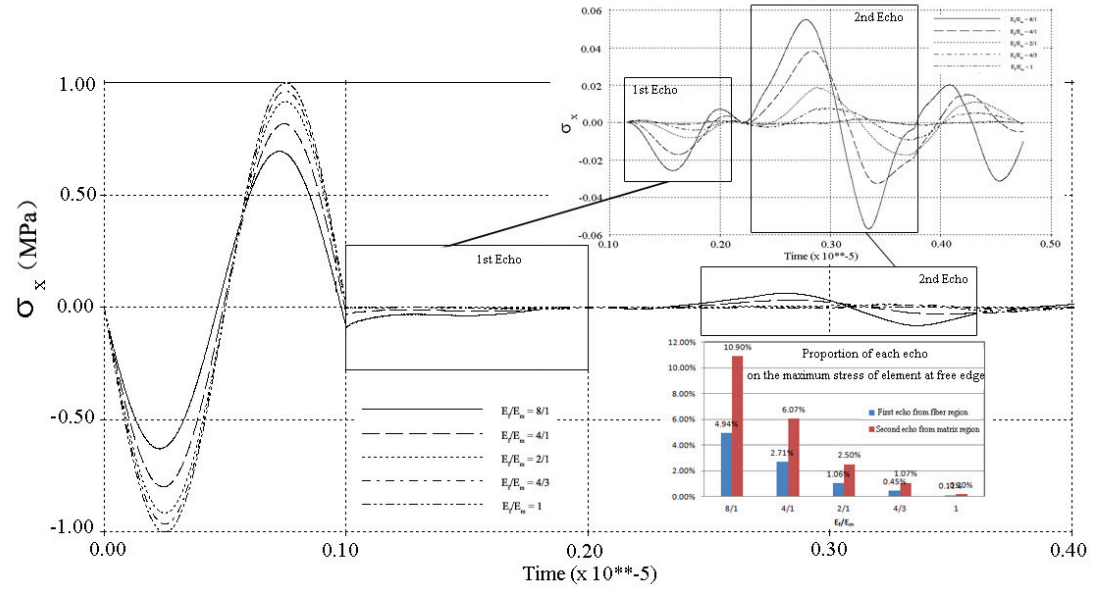

b) Variation of normal sterss of element at free edge in matrix region with different E_f/E_m

Fig.2-9 Stress wave form at the vicinity of free edge; Extracted scattering waves with different E_f/E_m.

The difference of σ_x between fiber region and matrix region becomes large as the E_f/E_m increased (anisotropic property to be obvious). Following the first cycle wave, there are several echoes (first echo and second echo, and so on) observed. Comparing with the model without defect, the reflection echo of 1st echo and 2nd echo can be extracted, which are shown in the inset of Fig.2-9. Based on the propagation time, the first echo in fiber region and the second echo in matrix region represents for the reflection wave from defect. The wave attenuation due to the mode conversion at interface resulted in the low reflection echo. Thus, from the inset of Fig.2-8, it can be seen that, when E_f/E_m=8, the stress value of first echo is only 1.67 % of the maximum stress value of incident wave, while in the matrix region, the maximum value of reflection echo is 10.9% of the incident wave. With the E_f/E_m decreasing to 1, the interlaminar shear still affect the wave propagation, which leads to the decrease of reflection echo. Hence, it is clear that, the interlaminar shear caused by the different propagation speed can significantly affect the wave propagation.

2.4.2.3 Stress Distribution at Defect Tips

When the ultrasonic wave propagates to the defect, the stress concentration occurs at the defect tips, and shows different distribution at different E_f/E_m. Here, the stress waveform of element near the defect tip is investigated, to know the correlation between

wave propagation and stress concentration at defect tips.

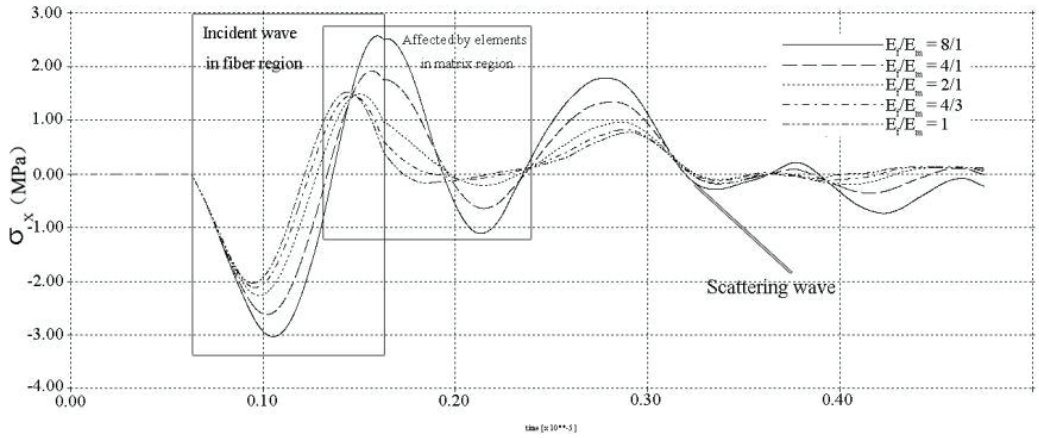

a) elements in fiber

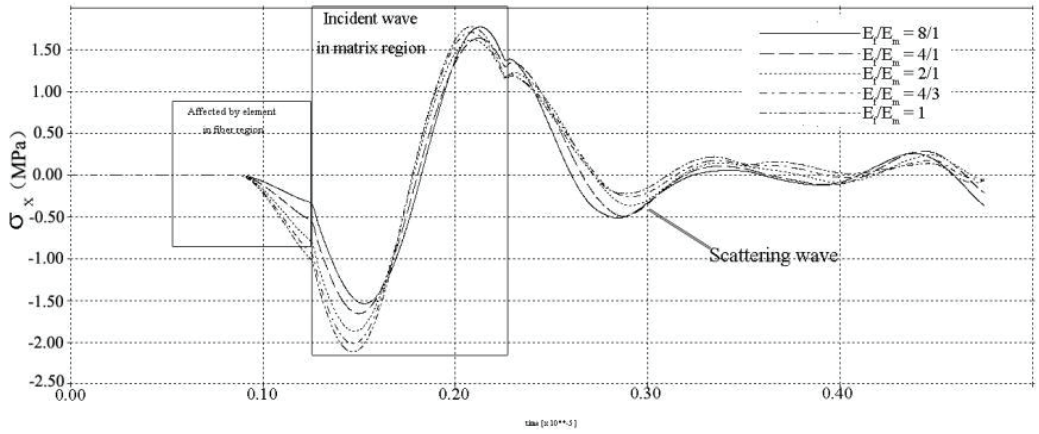

b) elements in matrix

Fig.2-10 Stress waveform at the defect tips with different E_f/E_m.

Fig.2-10 (a) exhibits the stress wave pattern in fiber region, where the incident waves from fiber region and matrix region and scattering wave from interface are distinguished by calculating the propagation time, and marked with the black rectangle. It can be seen that the waves from fiber and matrix region were superposed, which leads to the changing of peak value. In matrix region, as depicted in Fig.2-10 (b), the wave pattern is firstly

affected by the wave from fiber region. Then, a complete wave cycle can be seen, which is caused by the incident wave in matrix region. As a result, the waveform propagating at the defect tips become more complicated with irregular variation.

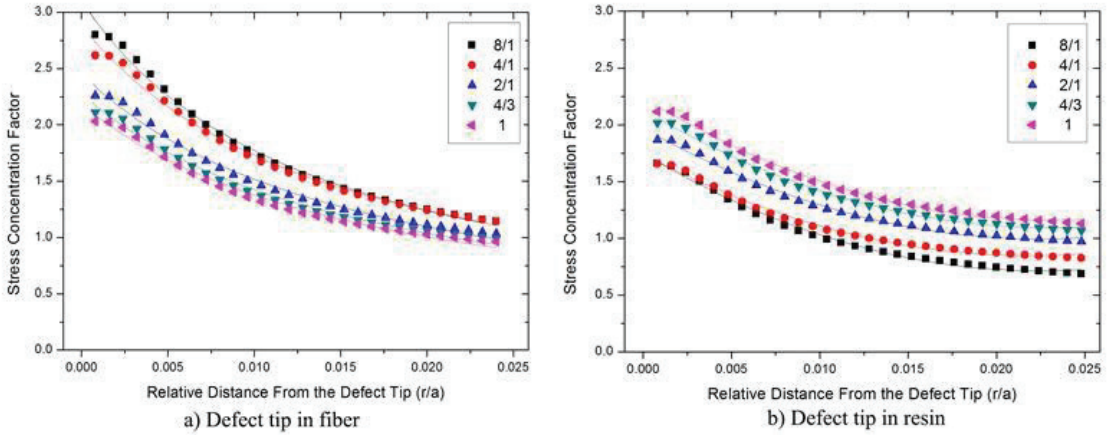

Fig.2-11 Normal stress distribution at defect tips with different E_f/E_m.

Table 2-3 Stress concentration at the defect tip for different E_f/E_m.

		Modulus ratio				
		8	4	2	4/3	1
Normal stress ratio	Defect tip in Fiber	3.55	3.08	2.52	2.44	2.43
	Defect tip in Matrix	2.09	1.97	2.02	2.49	2.51

Based on the maximum normal stress value of elements near the defect tip, the stress concentration at defect tips at fiber and matrix region are characterized, as shown in Fig.2-11. When E_f/E_m=1, the results of maximum stress value of defect tips at fiber and matrix

region gained here are in agreement with the theoretical value and this confirmed the validity of this method. With the E_f/E_m increasing to 8, the maximum stress value of defect tip in the fiber layer increased from 2.4 MPa to 3.6 MPa, whereas that in the matrix layer decreased from 2.5 MPa to 2.1 MPa. The influence of free edge effect and interface on the stress concentration at defect tips can be predicted by considering the wave propagation and its dynamic wave scatting. On the other word, by using the correlations between material property and ultrasonic wave propagation behavior, it is convenient to investigate the stress singularities and the dynamic variation of internal stress distribution in composite materials even with a failure region.

2.5 Conclusion

For bimaterial composite with ellipse-shaped defect, a new method combining stress distribution evaluation and ultrasonic propagation analysis is established. From this method, the correlation between ultrasonic wave propagation and stress singularities, dynamic stress distribution is investigated. It is clear that the material properties are closely related to the ultrasonic wave propagation. By changing the material property, with E_f/E_m changing from 1 to 8, the free edge effect and wave mode conversion at the interface become more remarkable. Since the resulting scattering waves caused by stress singularity at free edge and wave conversion at the interface, the ultrasonic propagation

behavior become more complicated. Using the dynamic waveform analysis during ultrasonic wave propagation, the stress echo from the free edge and interface and the influence of scatting wave are clarified. The stress concentration phenomenon at the defect tips with the influence of free effect and interface stress concentration are evaluated. The simulation results showed the method using ultrasonic wave propagation analysis is a convenient and effective way to evaluate the interaction between material properties, stress singularities and dynamic internal stress distribution in composite materials.

References

1. W. Sachse, B. Castagnede, I. Grabec, K.Y. Kim, R.L. Weaver, Ultrasnoics, 28 (1990) 97.
2. S.I. Rokhlin, W. Huang, Y.C. Chu, Ultrasnoics, 33 (1995) 351.
3. D. Datta, N.N. Kishore, NDT&E Int., 29 (1996) 213.
4. S. Biwa, S. Idekoba, N. Ohno, Mech. Mater., 34 (2002) 671.
5. N.W. Klingbeil, J.L. Beuth. Eng. Fract. Mech., 66 (2000) 93.
6. X.M. An, Z.Y. Zhao, H.H. Zhang, L. He, Eng. Anal. Boundary Elem., 37 (2013) 464.
7. J.J. Chang, C.L. Zheng, Q.Q. Ni, Compos. Struct., 75 (2006) 451.
8. N.J. Pagano, Int. J. Solids Struct., 14 (1978) 385.
9. N.J Pagano, Int. J. Solids Struct., 14 (1978) 401.

Chapter 3

Quantitative Evaluation of Ultrasonic Wave Attenuation components in Bimaterial Composites with Defect

Chapter 3: Quantitative Evaluation of Ultrasonic Wave Attenuation components in Bimaterial Composites with Defect

3.1 Introduction

When ultrasonic waves propagate in FRP composite materials, the propagation behaviors encompass not only characteristics of incident ultrasonic wave characteristics, features of microstructures and internal defects, but also information about the material anisotropy and viscoelasticity, even the interfacial condition between fiber and matrix. A much more detailed understanding about the ultrasonic wave propagation and attenuation characteristics is extremely important for the development of high precision ultrasonic technologies. However, for different individual wave components and corresponding attenuation components, different factors have different impacts. From the waveforms containing all coupling interactions of factors mentioned above, investigating the detailed mechanism of each effect factor independently is difficult but necessary. Thus, the key issue is to establish a method which can extract each individual attenuation component and then, clarify the variation behaviors with changing effect factors.

In the field of nondestructive testing for composite material, ultrasonic attenuation is an important subject, especially the scattering attenuation due to internal microstructures and defects, which has been studied by various researchers. For the composition of overall

ultrasonic wave attenuation, Beltzer et al [1] put forward a formulation of ultrasonic wave attenuation, in which the energy loss during the propagation is in terms of the wave scattering due to the inclusions and the attenuation property of the matrix. Together with Brauner [2], they studied the multiple scattering effects by means of investigating the independent scattering waves, and proposed the theory for evaluating the absorption and scattering attenuation components. For fiber reinforced composite materials with defects, the influence mechanisms of content or dimension of distributed defects/voids were well discussed. B.G. Martin [3] investigated the ultrasonic attenuation due to voids and obtained the expressions for ultrasonic attenuation as a function of both void and fiber content. By using the laser-ultrasonic spectroscopy method, Karabutov et al [4] investigated the influence of defect fractions and dimensions on the ultrasonic attenuation properties. With consideration of material viscoelasticity and the interrelation with incident wave frequency, Biwa [5-6] established a theoretical model for investigating the scattering attenuation and absorption in the composite in terms of the scattering and absorption cross-sections of independent inclusion and the matrix viscoelasticity. For the plain strain, time-harmonic problem of a layered material with single crack at the interface, based on the Green's integral theorem, Yang et al [7] analyzed the stress singularity around the crack and the scattering fields by using different material combinations. For

ultrasonic propagation in elastically anisotropic solids or combined materials, Yamawaki et al [8] proposed a simulation technique based on the improved nodal calculation method.

So far, there is still no well-defined model and solution which can systemically investigate each individual ultrasonic wave component and the corresponding attenuation components, with consideration of the spatial relation of defects, the interfacial interactions between constituent phases, and the influences of material anisotropy and viscoelastic property. Thus, we proposed a new approach on the base of time-domain finite element analysis of ultrasonic wave propagation, in which all individual attenuation components can be extracted from the overall attenuation and detailedly evaluated. In the approach, on the basis of the two-layer composite material model with an elliptical defect which was established in previous chapter, the ultrasonic wave propagation process, especially the shear stress waves, and the dynamic stress distribution are investigated, with consideration of material anisotropy. In order to extract the individual attenuation components, variant sub-models are also made by means of removing the interfacial defect, changing the fiber/matrix interface boundary conditions, and altering the matrix viscosity. By calculating the oscillating element energy, energy loss of above models are calculated, then the proportion of each individual attenuation component in overall attenuation characteristics are discussed. Here, we emphasize on the influence mechanism

of material anisotropy and viscoelastic property, while the other factors, such as incident wave frequency and dimension of defect, are hold constant, which allows the correlations between material properties and ultrasonic wave attenuation characteristics to be clarified.

3.2 FEM model

Herein, the 2-D 2-layered FEM model in chapter 2 is also utilized for representing the bimaterial composite, which is in the plane strain condition [9-11]. The same geometric sizes are selected: L=2h=10λ (λ, minimum wavelength of incident wave). When an ultrasonic wave propagates in an isotropic media, by introducing the longitudinal and transverse wave velocity, C_L and C_T, the ultrasonic wave equations of motion for two-dimensional plane strain in an isotropic media [12-13] are:

$$\begin{cases} c_L^2 \dfrac{\partial^2 u_x}{\partial x^2} + c_T^2 \dfrac{\partial^2 u_x}{\partial y^2} + (c_L^2 - c_T^2) \dfrac{\partial^2 u_y}{\partial x\, \partial \mathrm{y}} = \dfrac{\partial^2 u_x}{\partial t^2} \\ c_L^2 \dfrac{\partial^2 u_y}{\partial y^2} + c_T^2 \dfrac{\partial^2 u_y}{\partial x^2} + (c_L^2 - c_T^2) \dfrac{\partial^2 u_x}{\partial x\, \partial \mathrm{y}} = \dfrac{\partial^2 u_y}{\partial t^2} \end{cases} \tag{1}$$

where ρ is density. Eq.(1) indicates the direct correlation between wave velocity and ultrasonic wave propagation behavior. Therefore, the fiber and matrix region in presented bimaterial composites model are distinguished by specifying the density, longitudinal and transverse wave velocity, rather than specifying the elastic modulus of individual region. In the present model, the two regions are perfectly bonded by assigning the boundary conditions of interface to be fixed, which means the wave energy can transmit through

the interface due to the interface interaction. The coordinates are placed at the free edge of the interface [14-15], where the point A is the origin of the coordinates and the x-axis is along the interface.

For ultrasonic propagation in matrix region, with consideration of both viscous and elastic properties, the Eq.(1) can be rewritten as:

$$\left(K + \frac{4}{3}G\right)\frac{\partial^2 u_x}{\partial x^2} + (\eta_v + \frac{4}{3}\eta_s)\frac{\partial^3 u_x}{\partial t \partial x^2} = \rho\frac{\partial^2 u_x}{\partial t^2} \quad (2)$$

$$G\frac{\partial^2 u_y}{\partial x^2} + \eta_s\frac{\partial^3 u_y}{\partial t \partial x^2} = \rho\frac{\partial^2 u_y}{\partial t^2} \quad (3)$$

Eq.(2) and Eq.(3) respectively denote the longitudinal and shear waves, where *K* is the bulk modulus, and *G* is the shear modulus. η_v is for the bulk viscosity, and the η_s is the shear viscosity coefficient. In above two equations, the first term on the left-hand denotes the elastic component which is set by the velocity of wave propagation and the material density, the second term indicates the viscous component. By introducing the viscoelastic attenuation into matrix region and specifying the attenuation coefficient, the viscosity of matrix can be determined. The material properties for each individual region are as the same in chapter 2 [13].

The boundary condition of the model and the incident stress wave characteristics are assigned to be the same as that in chapter 2. The following sub-models are also built for extracting and evaluating the individual attenuation components, i.e. viscoelastic

attenuation, wave scattering attenuation and the energy loss at interface:

- Sub-model 1: no defect but with consideration of the viscoelastic attenuation of the matrix;
- Sub-model 2: with a defect but without consideration of the viscoelastic attenuation of the matrix.

Based on the above models, the ultrasonic wave propagation analysis is carried out by using the dynamic explicit finite element method.

3.3 Evaluation of Attenuation Components

From the classic description about the wave attenuation in composite materials with internal defects [2-5], matrix viscosity and the wave scattering due to the internal microstructures or defects are the major components in overall ultrasonic wave attenuation. However, in the present bimaterial structure, the perfect bonded interface and different material properties lead to interactions between fiber and matrix regions [16-17], which result in the energy dissipation at interface. Thus, the total energy loss rate $\langle I^{SUM} \rangle$ of the plane wave in the direction of ultrasonic wave propagation can be written in the form:

$$\langle I^{SUM} \rangle = \frac{d\langle e \rangle}{dx} = -\left(\langle I^{VIS} \rangle + \langle I^{DEF} \rangle + \langle I^{INT} \rangle \right) \tag{4}$$

where $\langle e \rangle$ is the time-averaged energy flux density, and $\langle \mathrm{I}^{VIS} \rangle$ is the energy loss rate

refer to matrix viscosity. $\langle \mathrm{I}^{DEF} \rangle$ and $\langle \mathrm{I}^{INT} \rangle$ represent for the wave scattering loss rate due to defects, and energy dissipation at fiber/matrix interface, respectively. From Biwa's work on the approximation of individual attenuation components [2], each component of energy loss rate in Eq.(4) can be derived as:

$$\begin{cases} \langle I^{VIS} \rangle = 2(1-\emptyset)\alpha^{VIS}\langle e \rangle_0 \\ \langle I^{def} \rangle = 2\alpha^{DEF}\langle e \rangle_0 \\ \langle I^{int} \rangle = 2\alpha^{INT}\langle e \rangle_0 \end{cases} \tag{5}$$

where $\langle e \rangle_0$ denotes the initial plane-wave energy flux density since the ultrasonic waves were incident into the model. α^{DEF} is the attenuation coefficient for wave scattering loss and α^{INT} is the attenuation coefficient due to the energy loss at fiber/matrix interface. α^{VIS} is the viscoelastic attenuation coefficient results from the specified matrix viscoelastic attenuation, which shows dependence of frequency. For eliminating the influence of frequency, the matrix viscosity is held constant by both specifying the attenuation coefficient and the corresponding frequency. $\emptyset$ represents the defect volume fraction (because our model is 2-D, we use here the area percentage of defect area).

Then, Eq.(5) was substituted into Eq.(4) and yield a first-order ordinary differential equation for $\langle e \rangle x$. From its solution, the attenuation coefficient of the composite α^{SUM} can be obtained. Herein, the material anisotropy is also taken into consideration as an important variable [17-18], and the modulus ratio, $\mu = E_f/E_m$, which represents for the

material anisotropy, was introduced into α^{SUM}:

$$\alpha^{SUM}(\mu) = (1 - \emptyset)\alpha^{VIS}(\mu) + \alpha^{DEF}(\mu) + \alpha^{INT}(\mu) \quad (6)$$

With consideration of the general composite materials such as GFRP, the Young's modulus ratios of fiber and matrix region, μ, is assigned to vary from 1 to 8. Herein, extracting individual attenuation components from the overall wave attenuation is the main issue. However, the interface interactions can affect the wave propagation in both fiber and matrix regions, as long as the fixed boundary condition of fiber/matrix interface exists, which result in the inseparable of α^{INT} when evaluating α^{VIS} and α^{DEF}. Hence, the elimination of α^{INT} is a key issue for extracting individual attenuation components. Herein, by introducing the roller support into interface bonding condition between the fiber and matrix region, the constraints between fiber and matrix region along the direction of interface are removed, and the interfacial shear stress can be zero. This means the wave propagation in the fiber and matrix regions are independent. Thus, the viscoelastic attenuation component, α^{VIS}, and the scattering energy loss from the defect, α^{DEF} can be calculated without the influence of interface interactions. Based on Eq.(6), we extract each individual attenuation components and then discuss the detailed effects of material anisotropy and matrix viscosity.

3.4 Results and Discussion

3.4.1 Extraction of Viscoelastic Attenuation Component

First, the variation behavior of viscoelastic attenuation with matrix viscosity and material anisotropy will be discussed. From Eq.(6), by removing α^{INT} and α^{DEF}, the viscoelastic attenuation can be separately evaluated. Thus, the defect-free model is used here for making the α^{DEF} to be 0. As mentioned above, the viscoelastic attenuation component is generated by the matrix viscosity, which is specified by the viscoelastic attenuation. In order to eliminate the influence of interface interactions, roller support has been introduced into the fiber/matrix interface to replace the original bonding condition, which result in the α^{INT} to be 0. The variation behavior of viscoelastic attenuation coefficients with material anisotropy and matrix viscosity are depicted in Fig.3-1(a). It can be seen that, with the increased matrix viscosity, the effects of material anisotropy on the increment of α^{VIS} in the present bimaterial composites became more significant. When matrix viscoelastic attenuation is 40dB/cm, with the modulus ratio increase from 1 to 8, α^{VIS} shows nearly 4 times increment in value. When matrix viscoelastic attenuation is at the range of 0 to 30 dB/cm, α^{VIS} also grow significantly. But beyond this range, it seems the influence of matrix viscosity become weaker, no obvious change of α^{VIS} can be seen.

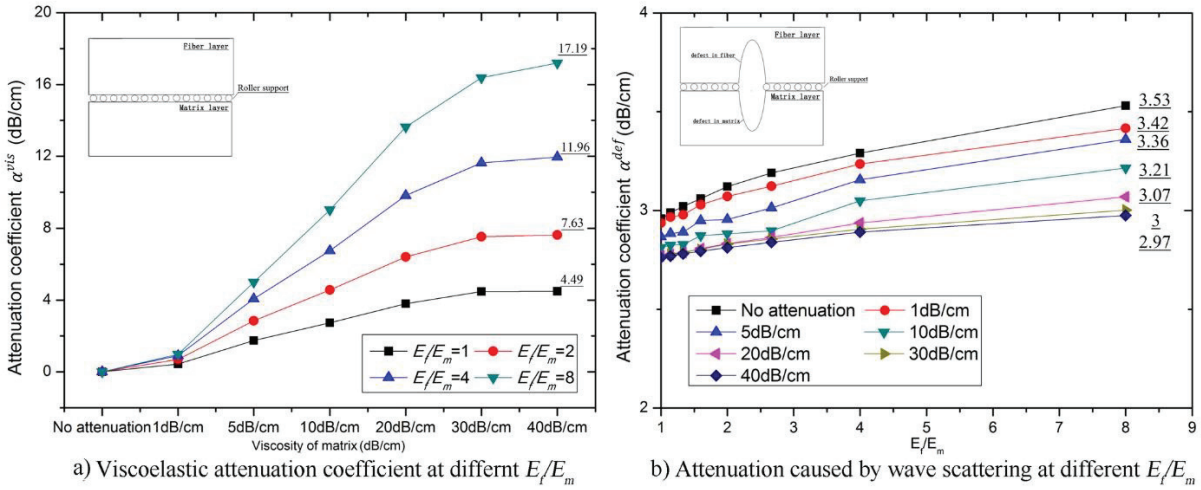

a) Viscoelastic attenuation coefficient at differnt E_f/E_m b) Attenuation caused by wave scattering at different E_f/E_m

Fig.3-1 The viscoelastic attenuation α^{vis} and the scattering attenuation α^{def} at different E_f/E_m.

3.4.2 Extraction of Scattering Attenuation Component

Then, the energy dissipation due to wave scattering from the transverse defect is discussed. The base model is used here, and the roller support is also introduced into the interface between the fiber and matrix region to keep α^{INT} to be 0. From Eq.(6), without calculating the scattering cross-section, the scattering attenuation due to the transverse defect, α^{DEF}, can be extracted by subtracting the viscoelastic attenuation energy, α^{VIS}, from the total energy loss, α^{SUM}. The variation behaviors of α^{DEF} with modulus ratio and matrix viscoelastic attenuation are evaluated, the results are shown in Fig. 3-1(b). It can be seen that, when E_f/E_m =1 and matrix with no viscosity, the scattering attenuation coefficient is 2.96 dB/cm, which is in agreement with results from a pure matrix with an elliptical defect. The scattering attenuation coefficients increase with the modulus ratio.

But comparing the variation of α^{VIS}, the increment of α^{DEF} is small, which is stems from the limited influence of material anisotropy on scattering losses at defects. The scattering wave attenuation mainly depends on the scattering cross-section of the defect [6].

The higher matrix viscoelastic attenuation means lower stress value during the ultrasonic wave propagation, which also corresponds to weaker scattering waves and lower scattering attenuation. With the viscoelastic attenuation of the matrix increased from 0 to 40 dB/cm, the scattering attenuation coefficients decrease. For example, when modulus ratio is 8, with the introduced matrix viscosity increased from 0 to 40 dB/cm, the wave scattering attenuation component decrease from 3.5 dB/cm to 2.97 dB/cm, which shows a relative larger variation than that under changing material anisotropy. Thus, it is clear that the influence of matrix viscosity on the scattering attenuation component is more influential than that of material anisotropy.

3.4.3 Extraction of Energy Loss at Fiber/matrix Interface

We now focus on the component of ultrasonic attenuation caused by the interface interactions, which combines the influence of the free edge effect and mode conversion at fiber/matrix interface. When ultrasonic wave loading is applied on the left side of the model (see Fig. 2-1), because of the different elastic modulus and the fixed fiber/matrix interface, a stress singularity occurs at the free edge, which is known as a “free edge effect”

[19−20].

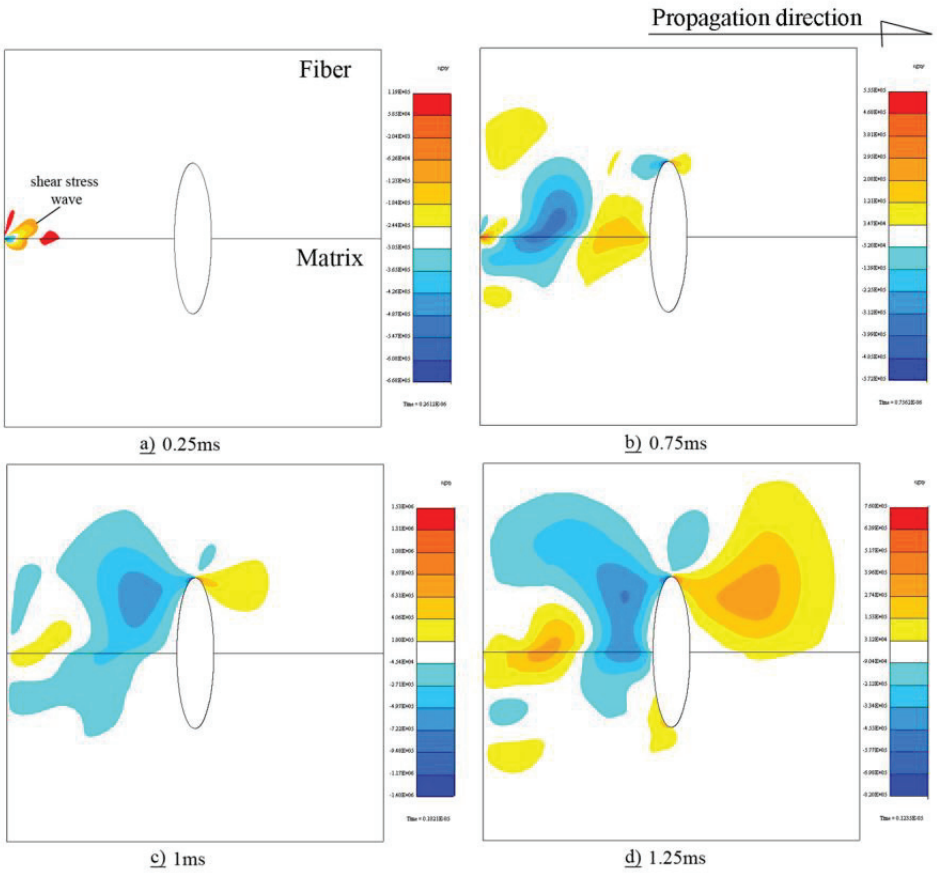

Fig.3-2. Shear stress wave propagation pattern at E_f/E_m=4.

The dynamic internal stress redistribution can be obtained on the basis of elastic wave theory used in chapter 2, just as shown in Fig.3-2, in which the shear stress distribution of the sample of E_f/E_m= 4 during the wave propagation within 1.25 ms were depicted. In Fig.3-2(a), it can be seen that, the wave mode conversion first generate at the free edge. Because of the stress difference between fiber and matrix region, the interface stats to bend, and interfacial shear stress generates at the free edge. As the ultrasonic wave

propagates beyond the free edge, the different arrival time of waveform fronts also results in interfacial shear deformation, and causes wave mode conversion at interface. As shown in Fig.3-2(b), shear stress waves spread asymmetrically in the region of the fiber/matrix interface ahead of the transverse defect. Then, shear stress waves further widens at the tips of the defect (Figs.3-2 (c) and (d)). In this process of wave mode conversion, the ultrasonic wave energy dissipates generally.

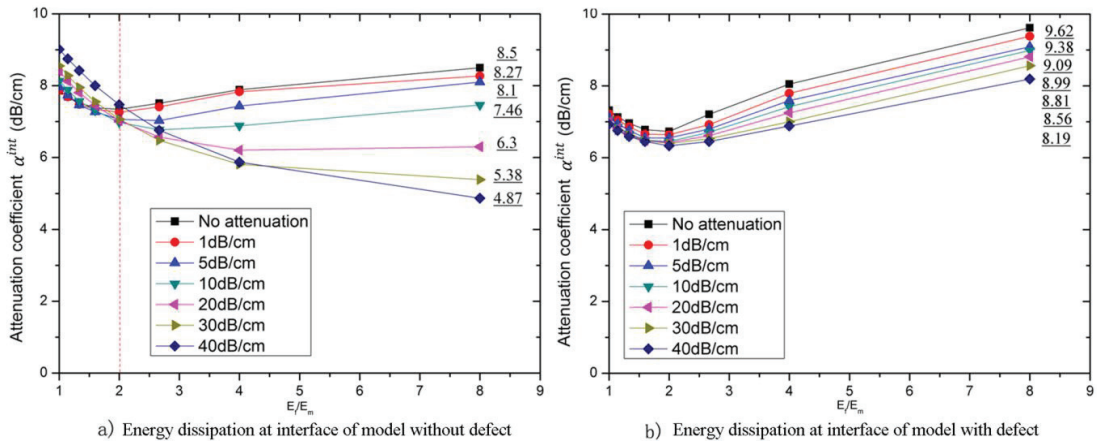

Fig.3-3. Energy dissipation at fiber/matrix interface under different E_f/E_m.

By subtracting the viscoelastic attenuation and scattering attenuation independently obtained in previous sections, α^{INT} can be calculated. And certainly, we also obtained the variation behavior of α^{INT} with different modulus ratio and matrix viscosity, as shown in Fig. 3-3 (a) and (b) (for model with and without transverse defect, respectively). For the model without defect, when the value of introduced matrix viscoelastic

attenuation coefficient is low, due to the weak influence of matrix viscosity on stress distribution at fiber/matrix interface, the interactions between fiber and matrix region become stronger with modulus ratio increased from 1 to 8, which results in an increasing energy dissipation at interface. When the matrix viscoelastic attenuation coefficient increased from 20 to 40 dB/cm, because of the significant influence of matrix viscosity on the wave propagation and the corresponding internal stress distribution, the interface interactions become weaker, which leads to the decrement of α^{INT} for E_f/E_m=1 to 8.

For models with transverse defect, as shown in Fig.3-3(b), unlike the variation behavior of model without defect, the value of α^{INT} become larger with increasing modulus ratio, whether the introduced matrix viscoelastic attenuation was low or larger. When the matrix viscoelastic attenuation is 40 dB/cm, the value of α^{INT} increased from 6.93 dB/cm to 8.19 dB/cm for models with defect, while it dropped from 9.01 dB/cm to 4.87 dB/cm in the model without the transverse defect. These can be explained by the influences of transverse defect on the stress distribution at fiber/ matrix interface, which will be discussed in the next section.

3.4.4 Shear Stress Distribution in Wave Propagation

Ultrasonic wave propagation is based on longitudinal and transverse waves, which are corresponding to normal and shear stresses respectively. In our analysis, the transverse

wave is generated from the wave mode conversion at fiber/matrix interface, and the scattering wave arises from the transverse defect, which corresponds to energy loss during the wave propagation. Thus, investigating the interfacial shear stress distribution under different material anisotropies and matrix viscosities is a way to confirm the ultrasonic attenuation mechanism in detail.

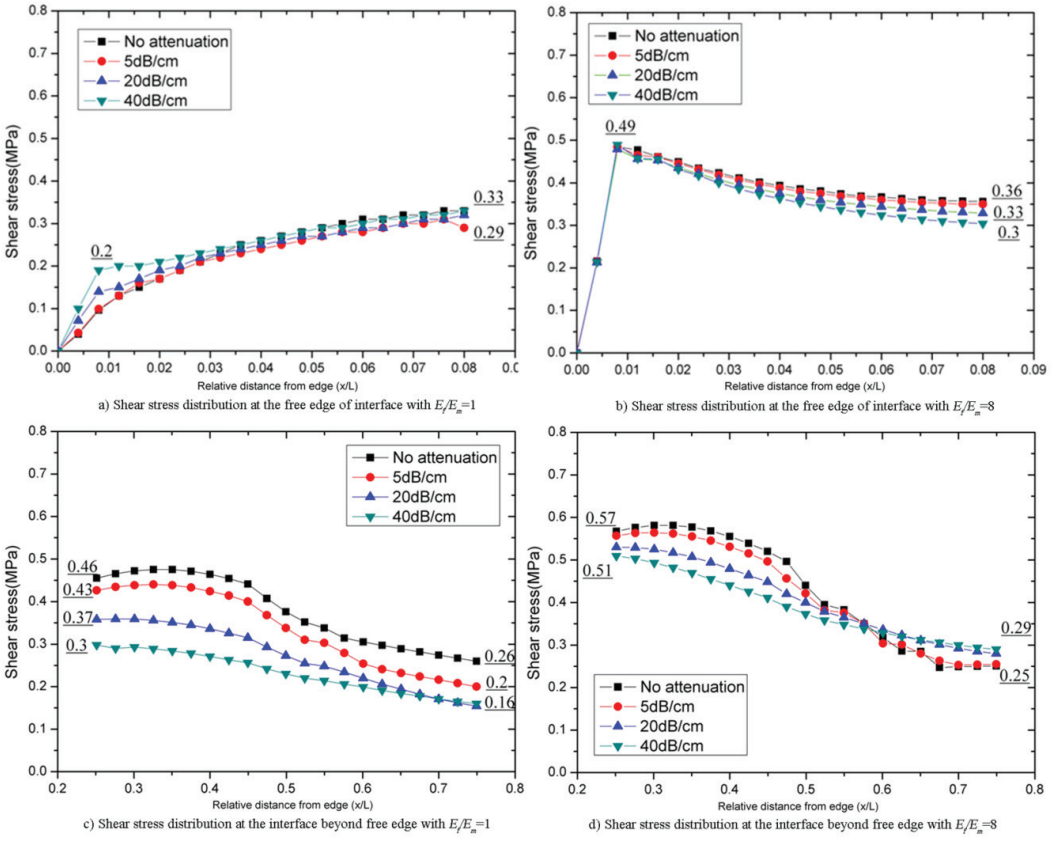

a) Shear stress distribution at the free edge of interface with E_f/E_m=1

b) Shear stress distribution at the free edge of interface with E_f/E_m=8

c) Shear stress distribution at the interface beyond free edge with E_f/E_m=1

d) Shear stress distribution at the interface beyond free edge with E_f/E_m=8

Fig.3-4 Shear stress distribution for model without defect at different E_f/E_m.

3.4.4.1 Models without interfacial transverse defect

Figs. 3-4(a) to (d) show the interfacial shear stress distributions in the models without

transverse defect but in different material anisotropy and matrix viscosity. In Figs.3-4(a) and (c), the modulus ratio is set to 1, while it is set to 8 in Figs.3-4(b) and (d). Because there is still no interlaminar stress difference since the ultrasonic wave loadings were applied on the left edge initially, the interfacial shear stress increase from 0. When ultrasonic waves propagate in the free edge region of models with low material anisotropy (E_f/E_m=1), as depicted in Fig.3-4(a), since the wave-front difference and the shear deformation between upper and lower region are both small, no shear stress concentration can be seen. As wave propagates, the ultrasonic waves in matrix region are spatially dissipated by the matrix viscosity, which results in the increment of interlaminar stress difference, and then the shear stress increase genially. And it can be seen that, the higher matrix viscosity dissipates more ultrasonic wave energy, and leads to a relative higher shear stress. For models with strong material anisotropy, as shown in Fig.3-4(b), due to the large shear deformation at free edge, a rapid raise of shear stress occurs at the free edge. When E_f/E_m=8 and matrix viscoelastic attenuation is 40 dB/cm, a peak of shear stress can be observed at the interface near the free edge with x/L=0.01(where x/L is the relative distance from the left edge), which is 0.49 MPa, almost 2.5 times larger than that at the same location when E_f/E_m=1. The materials anisotropic properties show an obvious influence on ultrasonic propagation and the corresponding internal stress distribution.

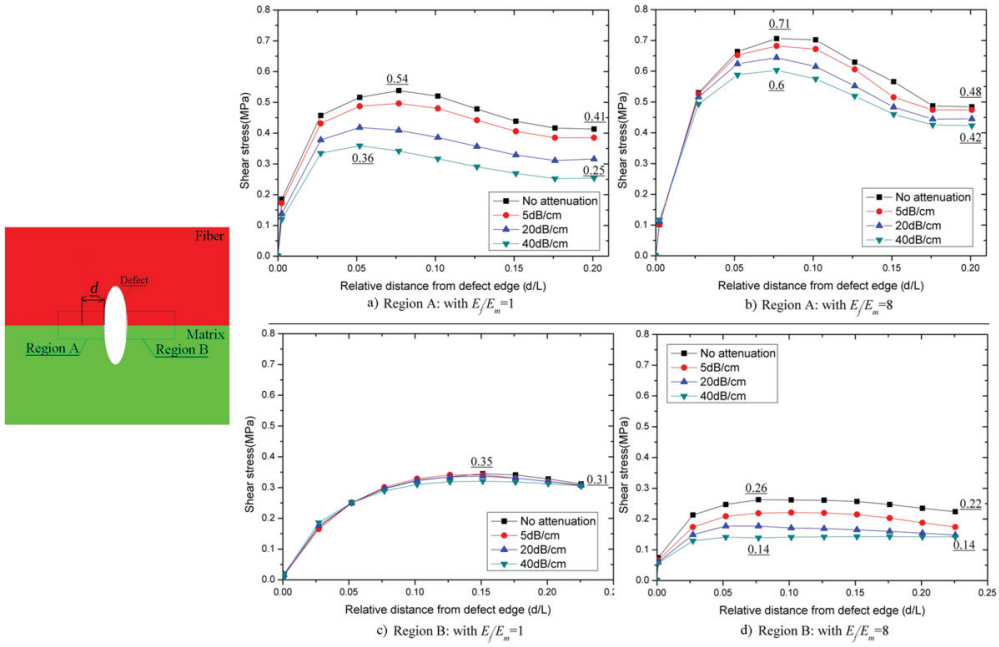

Fig.3-5 Shear stress distribution at the interface for models with defect at different E_f/E_m.

When ultrasonic wave propagates to the region beyond the free edge, as depicted in Figs.3-4(c) and d, the shear stress at fiber/matrix interface decreases because of wave energy dissipation refer to the matrix viscosity. And because more wave energy are dissipated in models with higher matrix viscoelastic attenuation, the shear stress values become lower as the matrix viscosity increased from 0 to 40 dB/cm. From the comparison of shear stress between E_f/E_m=1 and 8, the material anisotropic properties also have a significant influence on the shear stress distribution at the fiber /matrix interface beyond the free edge. When E_f/E_m=1 and matrix viscoelastic attenuation is 40 dB/cm, the reduction of shear stress value can be as much as 45 %, while a reduction of 51 % can be observed in models with E_f/E_m=8, the total shear stress levels generated are also much

larger.

3.4.4.2 Models with Interfacial Transverse Defect

For the models with transverse defect, the variation of shear stresses is depicted in Fig.3-5. Herein, the characteristics of the shear stress distribution can be observed in three regions: the free edge, the region before the defect (region A), and the region beyond the defect (region B). Because the free edge effect influences only the region near the free edge, we can consider the shear stress distribution in this region for model with transverse defect is the same as that for models without defects.

Figs.3-5(a) and (b) depict the curves of shear stress vs. relative distance from defect edge in region A, for models with different material anisotropy and matrix viscosity. The peak value of shear stress occurs at the location where the relative distance from defect edge in the direction of interface is in the range of 0.05-0.07. As same as the shear stress distribution in the free edge region, the reduction of shear stress with the increment of matrix viscosity can still be seen, and due to the relative greater shear deformation in model with high anisotropy, the total shear stress levels are also much larger when E_f/E_m=8.

However, in region B, compared with E_f/E_m=1, the total shear stress level for E_f/E_m=8 become lower. In Figs.3-5(c) and (d), the shear stress is reduced by 56 % at most when

the introduced matrix viscoelastic attention is 40 dB/cm. It can also be seen that the influence of the matrix viscosity on models when E_f/E_m=1 is not as obvious as that of models when modulus ratio is 8. Here we can confirm again that both matrix viscosity and material anisotropy can affect the shear distribution at the fiber/matrix interface, which results in variation in the interface interactions. Clearly, a relative stronger material anisotropy lead to more energy dissipation at interface, while the higher matrix viscosity always leads to less interfacial energy loss than that of models with low matrix viscosity.

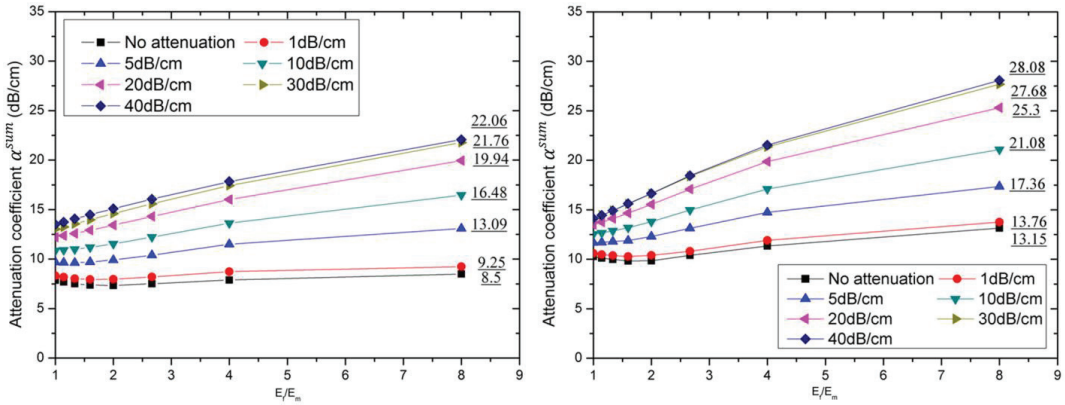

a) Overall attenuation of model without defect

b) Overall attenuation of model with defect

Fig.3-6 Overall attenuation coefficients of models with/without defect.

3.4.5 Quantitative Evaluation of the Overall Attenuation Composition

The variation behavior of overall attenuation coefficients against modulus ratio and matrix viscosity for models with and without defects are depicted in Fig3-6. Due to the influence of wave scattering from transverse defect, the overall attenuation for models

with defect shows a higher value than that of models without defect. From inspection of Fig.3-6, each line shows a tendency to increase with the viscoelastic attenuation of the matrix, as well as the modulus ratio, E_f/E_m. For example, for the case of a constant matrix viscoelastic attenuation of 40 dB/cm, when E_f/E_m changed from 1 to 8, the total attenuation coefficient α^{SUM} without a defect increases from 13.5 to 22.06 dB/cm, about a 8.5 dB/cm increment; while the total attenuation coefficient α^{SUM} with the defect increases from 14.11 to 28.08 dB/cm, an approximately 14 dB/cm increment. In the case of the constant material anisotropic property of E_f/E_m=8, when the matrix viscoelastic attenuation changed from 0 to 40 dB/cm, the total attenuation coefficient α^{SUM} without the defect increases from 8.5 to 22.06 dB/cm, nearly a13.5 dB/cm increment; while it increases from 13.15 to 28.08 dB/cm, an approximately15 dB/cm increment, for the model with transverse defect.

3.4.5.1 Models without Interfacial Transverse Defect

In Figs.3-7(a) and (d), the proportions of each attenuation component in overall attenuation are depicted for the composite materials models without defects. When the matrix viscoelastic attenuation coefficient is 0 dB/cm, the overall attenuation is only caused by interface interactions, or, in other words, the proportion of α^{INT} is 100 %.

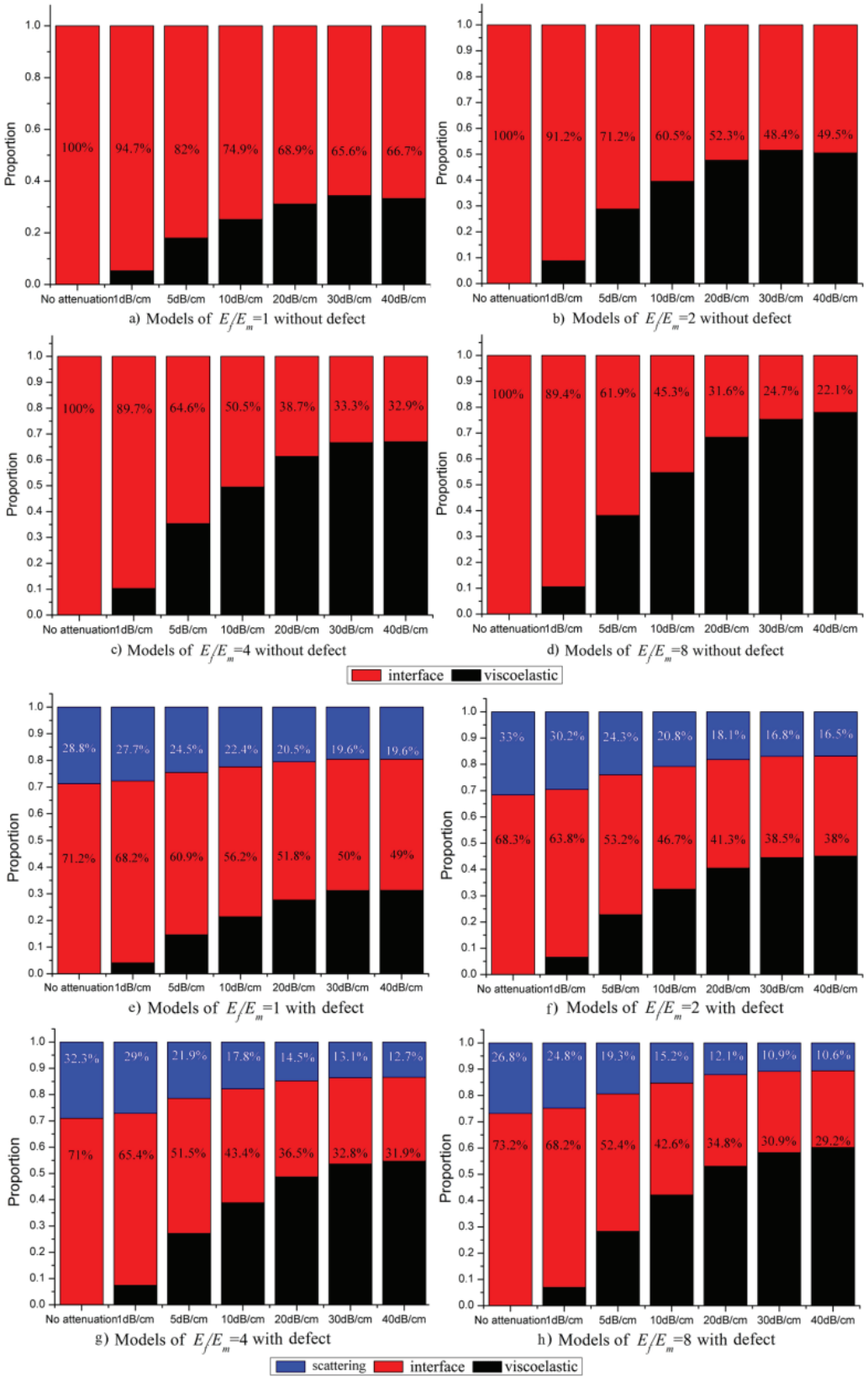

Fig.3-7 Proportion of each attenuation components for models without/with defect.

As the material anisotropy becomes stronger, the wave energy dissipation due to material viscoelastic properties and interface interactions both increase. However, because of the relative greater increment of viscoelastic attenuation, the proportion of the interface interaction attenuation decreases. When the matrix viscoelastic attenuation coefficient is below 5 dB/cm, the main part in overall attenuation is caused by interfacial interactions. For instance, the contribution of α^{INT} increases from 61.9 % at E_f/E_m=8 to 82 % at E_f/E_m=1. When the matrix viscoelastic attenuation increases from 10 dB/cm to 40 dB/cm and the modulus ratio is low, as mentioned in previous section, the matrix viscosity gives weak influences on the shear stress distribution at interface. Although the introduced matrix viscoelastic attenuation increases from 5 dB/cm to 40 dB/cm, the energy loss at interface is still the main part. It can be seen that the contribution of α^{INT} decreases from 60.5 % to 49.5 % with the introduced matrix viscoelastic attenuation increases from 10 dB/cm to 40 dB/cm. On the contrary, when the modulus ratio increases from 2 to 4, the interfacial interactions are remarkably reduced by matrix viscosity. This reduction of energy loss at interface resultes in the increment of α^{VIS}. For instance, when E_f/E_m=8, with the matrix viscosity changes from 10 dB/cm to 40 dB/cm, the contribution of material viscoelastic attenuation component increased from 54.7 % to 77.9 %.

3.4.5.2 Models with Interfacial Transverse Defect

For models with transverse defect, as depicted in Figs.3-7(e) and (f), the main part of the overall attenuation is also the energy loss at interface, which shows a decreasing tendency as E_f/E_m and matrix viscoelastic attenuation are increased. When there is no viscoelastic attenuation introduced into the matrix region, the scattering attenuation component can provide as much as 33 % to overall attenuation. When viscosity is introduced into matrix region, the contribution of scattering attenuation component becomes lower. For instance, when modulus ratio is 2, the proportion of α^{DEF} in overall attenuation decreases from 33 % to 16.5 %, as the introduced matrix attenuation coefficient increases from 0 to 40 dB/cm. It can also be seen that, the viscoelastic attenuation can be a major component in overall attenuation when the material anisotropy and the matrix viscosity are both strong. Such as the case of E_f/E_m=8 and matrix viscoelastic attenuation is 40 dB/cm, the α^{VIS} can provide as much as 60.2 % to the overall attenuation. From the above studies, each attenuation component can be separately evaluated, and correlations between each individual attenuation components and the material properties, such as material anisotropy and viscoelastic property, are clarified.

3.5 Conclusions

Based on the time-domain finite element analysis for ultrasonic propagation in a two-layer fiber/matrix composite materials model with ellipse-shaped transvers defect, a new method is proposed, in which the individual attenuation components, including viscoelastic attenuation, wave scattering attenuation, and the interface interactions are separately investigated. The influence mechanism of material anisotropy and viscoelastic property on the wave propagation and attenuation characteristics are clarified, by means of investigating the variation behaviors of each individual components. The analysis of dynamic interfacial shear stress distribution demonstrate the tight correspondence between internal dynamic stress redistribution and ultrasonic wave attenuation characteristics, and applied in the investigation of influence mechanisms of interfacial defect, material anisotropy and viscoelasticity. The results showed that energy dissipation caused by interface interactions is a major part of the overall ultrasonic wave attenuation. Each attenuation component is closely related to the material anisotropy and matrix viscoelastic properties. The present method can be applied to the analysis of ultrasonic wave attenuation characteristics in both fiber- and particle- reinforced composite materials, and will provide strong support for the further development of high precision ultrasonic technologies.

References

1. A.I. Beltzer, C.W. Bert, A.G. Striz, Int. J. Solids Struct., 19 (1983) 785.

2. A.I. Beltzer, N. Brauner, Mech. Mater., 6 (1987) 337.

3. B.G. Martin, NDT Int. 9 (1976) 242.

4. A.A. Karabutov, N.B. Podymova, Composites Part B, 56 (2014) 238.

5. S. BIWA, Mech. Mater., 33 (2001) 635.

6. S. Biwa, Y. Watanabe, N. Ohno, Compos. Sci. Technol., 63 (2003) 237.

7. H.J. Yang, D.B. Bogy, Rev. Prog. Quant. Nondestr. Eval.,.5A (1986) 53.

8. H. Yamawaki, T. Saito, NDT&E Int., 33 (2000) 489.

9. P.B.N. Prasad, N. Hasebe, X.F. Wang, Y. Shirai, Int. J. Solids Struct., 42 (2005) 1513.

10. R. Chasudhuri, Compos. Struct., 72 (2006) 141.

11. R. Chasudhuri, Compos. Struct., 93 (2011) 513.

12. J.L. Rose, *Pres.* Cambridge University , London, (1999) 24.

13. J.J. Chang, C.L. Zheng, Q.Q. Ni, Compos. Struct., 75 (2006) 451.

14. F. Stenger, R. Chaudhuri, J. Chiu, Compos. Sci. Technol., 60 (2000) 2197.

15. L. Sebastien, A. Lhemery, P. Calmon, S. BIWA, Quant. Nondestr. Eval. 700 (2004) 875.

16. E.S. Folias, Int. J. Solids Struct., 25 (1989) 1193.

17. J. Dundurs, J. Compos. Mater., 12 (2010) 253.

18. S. Itou, Eng. Fract. Mech., 25 (1986) 475.

19. L.G. Pauline, P. Bernard, B. Mathias, D.S. Gery, S. Laurent, Composites Part A, 40 (2009) 1911.

20. R.Z. Chaudhuri, M.S. Xie, Compos. Struct., 40 (1998) 129.

Chapter 4

Analysis of Individual Attenuation Components of Ultrasonic Waves Considering Frequency Dependence

Chapter 4: Analysis of Individual Attenuation Components of Ultrasonic Waves Considering Frequency Dependence

4.1 Introduction

The frequency characteristics is also an important subject in nondestructively evaluation and characterization of fiber-reinforced composite material. On the basis of aforementioned method which can separately and quantitatively evaluate the ultrasonic wave attenuation, the frequency characteristics of each individual attenuation component under different combination of material viscosity and anisotropy are investigated, for gaining a better understanding of the detailed influence of effect factors mentioned in chapter 3.

A number of researches have been conducted to study the ultrasonic propagation behaviors and attenuation characteristics of fiber or particle reinforced composite material, with considering the frequency characteristics. Beltzer and Brauner [1] studied the frequency dependence of attenuation by means of a dynamic differential scheme based on energy attenuation analysis in a random fiber composite. In this method, the absorption attenuation caused by viscous nature of matrix and the energy loss caused by scattering were taken into consideration, although the frequency characteristics of the above attenuation components was not investigated. Karabutov and Podymova [2] investigated

the variation of ultrasonic attenuation with void fractions and incident wave frequencies but did not consider the matrix viscosity. Liu et al. [3] used the extended finite element method (FEM) to study the influence of fiber orientation and frequency on the attenuation characteristics. Although it was concluded that the greatest attenuation happens when the fibers are aligned in the direction of wave propagation, the detailed effect mechanism of fiber orientation on the attenuation components was not clear.

Here, based on the aforementioned method in chapter 3, each individual attenuation components are extracted from the overall attenuation and separately discussed under different material viscosity and anisotropy, and incident wave frequency.

4.2 Analysis Model and Formulations

4.2.1 FEM Base Model

Herein, we also utilize the 2-D bimaterial composite FEM model with elliptical transverse defect, and the sub-models as same as aforementioned in chapter 3 [4-5]. Based on the above models, the ultrasonic wave propagation analysis is carried out by using the dynamic explicit finite element method. Time-harmonic plane waves are also applied on the composite in the direction of the positive x axis, which are assumed to be one-cycle sinusoidal longitudinal wave with amplitude of 1 MPa.

4.2.2 Analysis of the Attenuation Components

From the classic description about the wave energy dissipation in fiber- or particle-reinforced composite materials with imperfections, matrix viscosity and the wave scattering due to the internal microstructures or defects are the major parts in wave attenuation characteristics. As discussed in the previous chapter, after the ultrasonic wave loading applied on the left surface, the interfacial stress appeared due to the perfect bonded interface and different material properties, and further propagate with the ultrasonic wave propagation. The interactions between interfaces dissipate the energy of incident waves [6-7]. Thus, the energy loss can be expressed as:

$$\langle I^{SUM} \rangle = \left(\langle I^{VIS} \rangle + \langle I^{DEF} \rangle + \langle I^{INT} \rangle \right) \tag{1}$$

where the superscript *DEF* indicates the scattering loss due to the defect, *VIS* indicates viscoelastic attenuation, and *INT* indicates energy loss at the fiber/matrix interface [8]. It is clear that, both of the material anisotropy and incident wave frequency can significantly alter the ultrasonic wave propagation behavior and internal stress distribution, result in the variation of individual attenuation components [9-10]. Hence, based on the Eq.(1), we obtain the overall attenuation coefficient, α^{SUM}, as a function of the modulus ratio, E_f/E_m, and the incident wave frequency, as follows:

$$\alpha^{SUM}(\mu, f) = (1 - \emptyset)\alpha^{VIS}(\mu, f) + \alpha^{DEF}(\mu, f) + \alpha^{INT}(\mu, f) \tag{2}$$

Based on Eq.(2), we extracted each individual attenuation components and then discuss the frequency characteristics of them.

4.3 Results and Discussion

4.3.1 Viscosity of the Matrix

As aforementioned in section 4.2, the viscosity of presented bimaterial model was exhibited by the matrix viscosity. It can affect the ultrasonic wave propagation in both fiber and matrix region via the perfect bonded interface, resulted in the variation of attenuation characteristics. Based on the extraction of attenuation components, by altering the introduced matrix viscoelastic damping, the variation behavior of attenuation coefficients of individual components can be studied. Herein, bimaterial composite models with their Young's modulus ratio, E_f/E_m, to be 8 were utilized. The viscoelastic attenuation of matrix was set to increase from 0 to 40 dB/cm corresponding to the incident wave frequency in 1 MHz. As shown in Fig.4-1, the viscoelastic attenuation of the two-layered composite material exponential increases with the matrix viscosity, reaching a maximum value of 17.19 dB/cm when the viscoelastic attenuation is 40 dB/cm. With the increase of matrix viscosity, the amplitude reduction during the ultrasonic wave propagation became larger, leads to weaker scattering waves and interface interactions, which finally results in the gradually drop tendency of the scattering attenuation and

energy loss at the interface. With the matrix viscosity increased from 0 to 40 dB/cm, the energy loss at interface decreased from 9.62 to 8.19 dB/cm. Because the wave scattering is mainly dependent on the dimension of the defect, the effect of matrix viscosity on the scattering attenuation is small (decreased from 3.53 to 2.98 dB/cm).

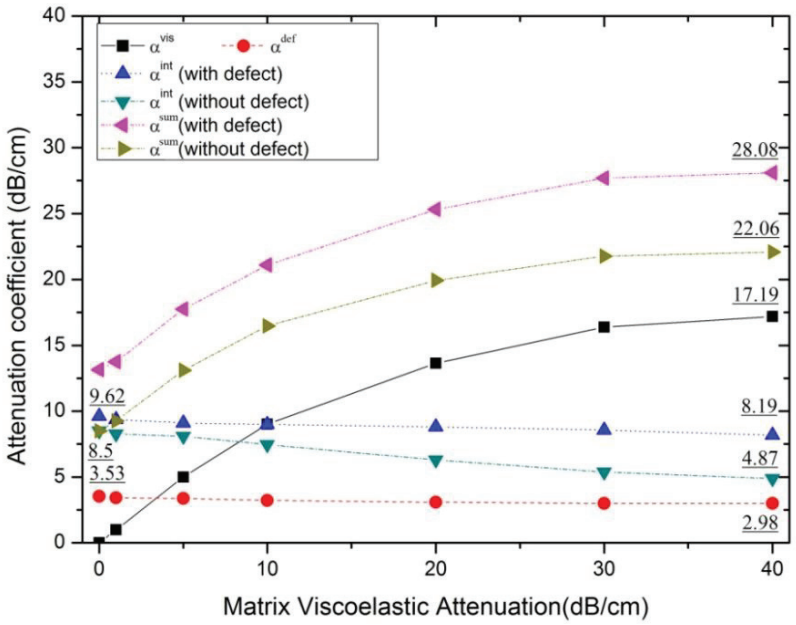

Fig.4-1 Variation of individual attenuation components with increased matrix viscosity for models with E_f/E_m=8 and the incident wave frequency of 1 MHz.

For comparison, the model without defect (sub-model 1) was also used. Because the presence of transverse defect can significantly affect the stress distribution around it [6-7], leads to the increase of interlaminar shear stress at the region of fiber/matrix interface near the defect, the energy loss at the interface for models with defect was greater than that in the model without a defect (up to 1.7 times when the matrix viscoelastic attenuation

is 40 dB/cm), while the decrease of α^{INT} for model without defect is more remarkable than that in the model with defect (approximately 3.6 dB/cm for model without defect, while it decreased 1.43 dB/cm of model with defect).

4.3.2 Incident Wave Frequency

Then, based on the extraction of attenuation components as aforementioned, the frequency characteristics of the individual attenuation components were evaluated.

For the present two-layered composite model, both of the fiber/matrix interface and the transverse defect can shift the frequencies of the incident ultrasonic waves [11], because of the scattering waves and wave mode conversion. From the definition of viscoelastic damping in the present model, when the wave frequency is above or below this frequency, the attenuation value will be lower, which is within about 80 % of the peak value in the range of $0.5 \times f_0$ to $2 \times f_0$, where f_0 is the specified frequency. These result in the change of corresponding viscoelastic attenuation in matrix region, and affect the stress distribution and the ultrasonic wave propagation at fiber/matrix interface. Therefore, the other attenuation components, i.e. scattering attenuation and energy loss at interface were also affected by the incident wave frequency. In order to investigate the frequency characteristics of each attenuation components, the Incident wave frequency was assigned to increase from 0.01 to 30 MHz. The Young's modulus ratio was also

assigned to 8, and the viscoelastic attenuation of matrix was specified as 20 dB/cm.

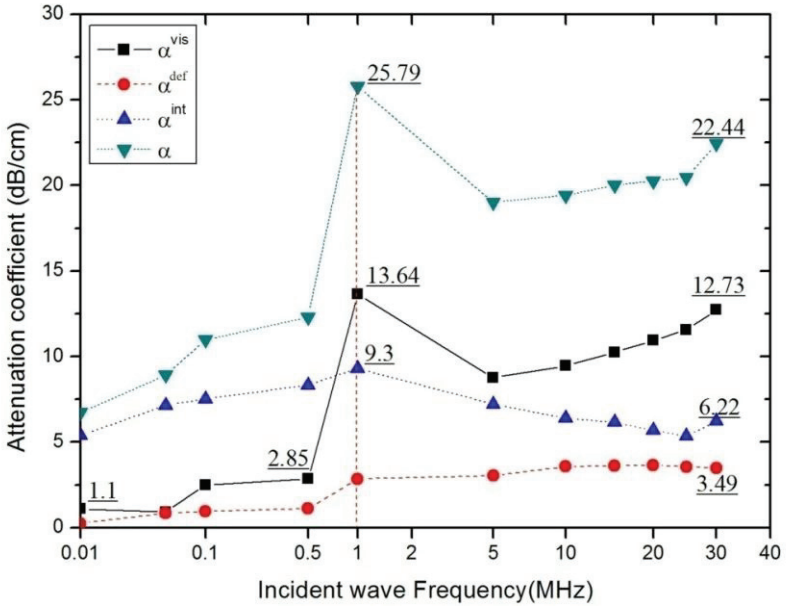

Fig.4-2 Variation of individual attenuation components with increased incident wave frequency for models with E_f/E_m=8 and the viscoelastic attenuation of matrix region of 20 dB/cm.

The results of the individual attenuation components under different incident wave frequencies were depicted in the Fig.4-2. It can be seen that, each attenuation component showed frequency dependence, especially the viscoelastic attenuation, α^{VIS}. With the increase of incident wave frequency, the attenuation coefficient, α^{VIS}, gradually increased, from 1.1 dB/cm at 0.01 MHz to 12.73 dB/cm at 30 MHz. A peak value can be seen at 1 MHz, which reached the maximum value of 13.64 dB/cm. This result of α^{VIS} is due to the obviously frequency dispersion caused by the scattering waves and mode conversion during the propagation in the basic model, which can be explained by the frequency

response of the present two-layered composite material.

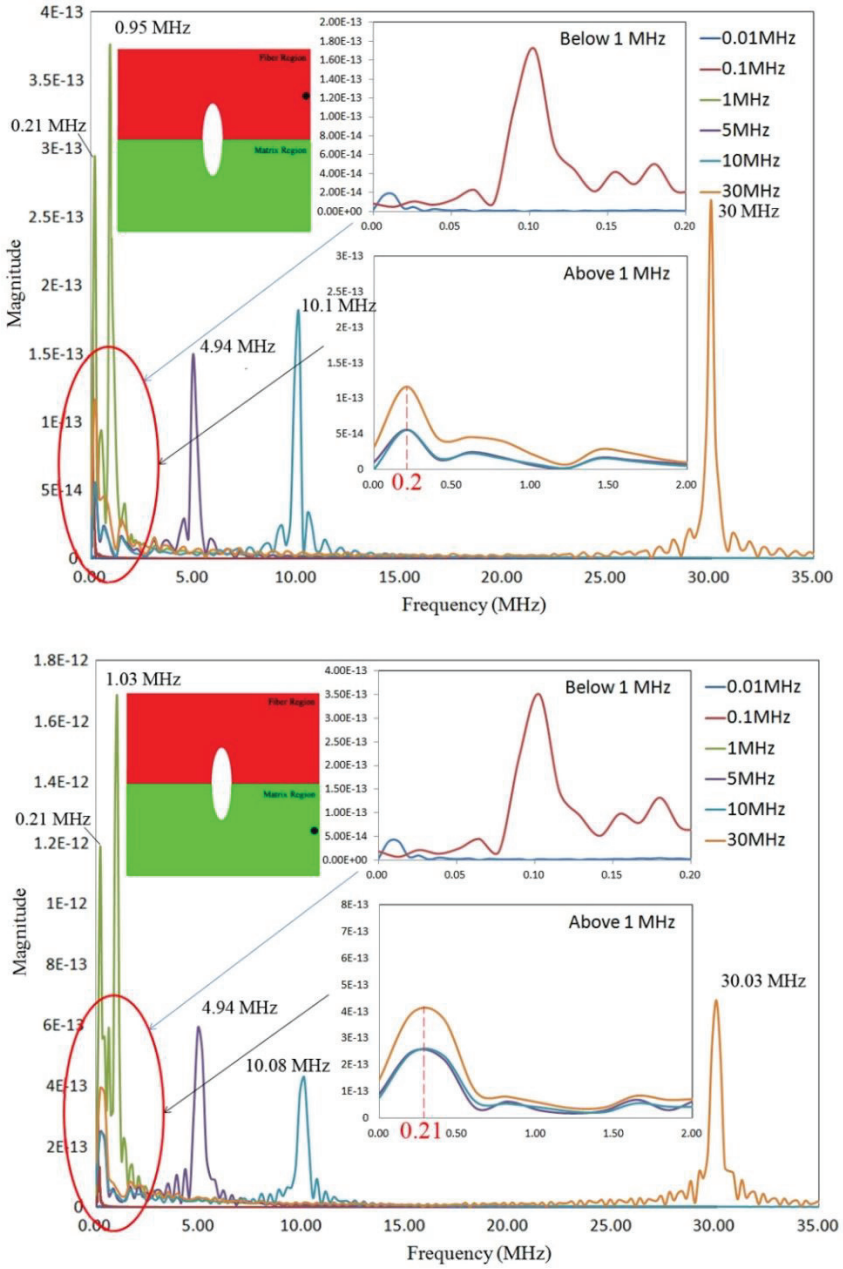

Fig.4-3 Frequency spectrum of the two-layered composite model under different incident wave frequencies.

By applying a small sinusoidal vibration load on this two-layered composite material (here, we used sub-model 2) with single frequency (increased from 0.01 to 30 MHz),

the displacement signals of elements from the right side in fiber and matrix region were proceed with FFT transformation respectively and the frequency spectrums of this two-layered system were obtained, as depicted in Fig.4-3. When the incident wave frequency increased from 1 to 30 MHz, due to the wave length became smaller than the defect size (the dimension of elliptical defect is defined as: $a = 2b = 2\lambda$, where the λ is the wavelength when the frequency is 1 MHz), wave scattering and mode conversion occurred and lead to the frequency dispersion during the ultrasonic propagation. When the frequency is 1 and 30 MHz, it can be seen that the spectrum peaks both appeared at 0.21 and 10.08 MHz. As aforementioned, the attenuation values becomes lower when the wave frequency is above or below this frequency. Therefore, the wide dispersion range results in the relative low viscoelastic attenuation at the range of 5 to 30 MHz.

Because the variation of matrix viscosity can significantly alter the stress distribution, the energy loss at the interface also represents frequency dependence. During the frequency range of 0.01 to 1 MHz, the weak viscosity of matrix results in relative stronger interlaminar shear, which leads to the relative larger energy loss at interface than the α^{VIS}. As depicted in Fig.4-2, the α^{INT} increased from 5.2 dB/cm to the peak value, 9.3 dB/cm at 1MHz. With the incident wave frequency increased from 1 and 30 MHz, the effect of the matrix viscosity on the ultrasonic wave propagation became remarkable, leads to the

decrease of interlaminar shear stress and less energy loss at the interface. The α^{INT} decreased from 9.3 to 6.2 dB/cm.

From the red dash line in Fig.4-2, the scattering attenuation, α^{DEF}, increased with increasing incident wave frequency. However, in comparison with α^{VIS}, the increment of α^{DEF} is small, which is stems from the scattering wave attenuation mainly depends on the dimension of the defect [8]. Therefore, for this two-layered composite material with transverse defect, the frequency characteristics of the individual attenuation components were measured, and the contributions of them to the overall attenuation were cleared.

4.3.3 Anisotropy of the Material

The material anisotropy is the main cause of interlaminar shear in the layered composite material. From the author's previous work, with the increase of the Young's modulus ratio, E_f/E_m, the interface bending deformation becomes larger, leads to the propagation direction change of ultrasonic waves at the region of fiber/matrix interface. The altered internal stress distribution then affects the attenuation characteristics. Herein, the Young's modulus ratio of fiber and matrix region, E_f/E_m, was assigned to be varied from 1 to 8 by altering the density of the matrix (the wave propagation velocity of the fiber and matrix were held constant), and the variation behavior of each individual

attenuation components with material anisotropy were investigated. The matrix viscosity was assigned to 20 dB/cm, and in order to analyze the coupling effect of the incident wave frequency, the incident wave frequency was assigned as 0.01, 0.1, 1, 10, and 30 MHz.

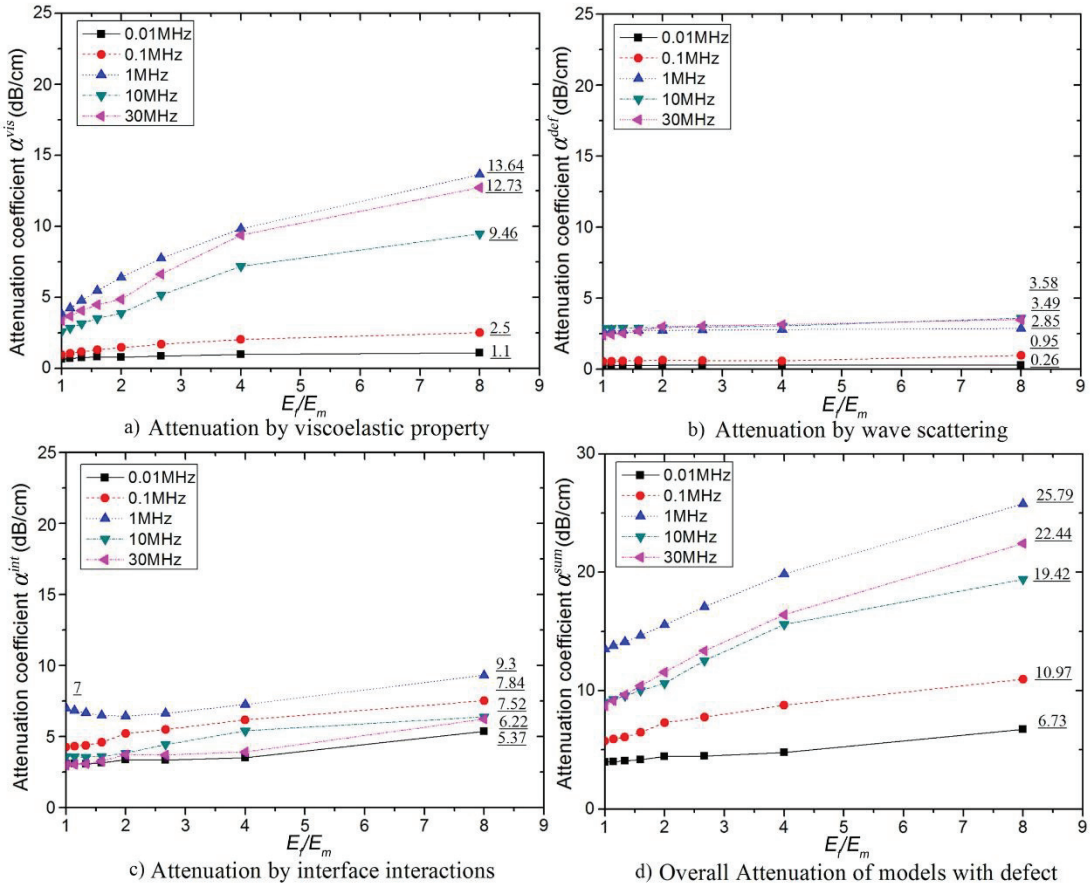

Fig.4-4 Variation of individual attenuation components with increased material anisotropy and incident wave frequency.

From the results of the individual attenuation components in Fig.4-4(a), the viscoelastic attenuation increased exponentially with the modulus ratio, μ. For example, at 0.01 MHz, the viscoelastic attenuation increased from 0.6 to 1.1 dB/cm; at 30 MHz, the viscoelastic attenuation increased 5 times, from 2.7 to 12.73 dB/cm. As presented in

the previous section of the frequency characteristics of viscoelastic attenuation, α^{VIS}gradually increased with the incident wave frequency, and the maximum value both occurred at 1 MHz. Because of the weak interface interactions when the E_f/E_m is small, the matrix viscosity has minimal effects on the wave propagation in fiber region, leads to the relative low value of attenuation coefficients and low growth with incident wave frequency. As depicted in Fig.4-4(a), at E_f/E_m=1, the α^{VIS} increased from 0.6 to 3.9 dB/cm. When the material anisotropy is strong, the significant interface interactions result in the obvious increase of α^{VIS}. When E_f/E_m=8, the α^{VIS} increased from 1.1 to 13.64 dB/cm.

The scattering wave is closely related to the dimension of defect, and the material anisotropy has little effect on it, as depicted in Fig.4-4(b). During the increase of the modulus ratio, the scattering attenuation coefficient increases, albeit to a much smaller extent than α^{VIS}. However, the scattering attenuation shows a strong frequency dependence, which increased 11 times when the frequency increased from 0.01 to 1 MHz at E_f/E_m=8. At 10 and 30 MHz, the influence of frequency becomes weak and the scattering cross-section of the defect is the main determinant of attenuation. In Fig.4-4(c), α^{INT} represents a more obvious change with the increase of material anisotropy than that of the scattering attenuation, due to the direct relation of matrix viscosity and the

interfacial stress distribution. When the Young's ratio was between 1 and 2, because of the weak interface interactions, the variation of the α^{INT} is quite small. When E_f/E_m is increased from 2 to 8, with the increase of interface interactions, the increment became larger.

The overall attenuation coefficients for models with defect under different combination of material anisotropy and incident wave frequencies are depicted in Fig.4-4(d). When E_f/E_m increased from 1 to 8, it is evident that the overall attenuation mainly represents the variation tendency of the viscoelastic attenuation and the energy loss at the fiber/matrix interface. From the above, the strong correlation between the material anisotropy, viscous property, incident wave frequency and the detailed attenuation characteristics can be clarified.

4.3.4 Contribution of Individual Attenuation Components

The contributions of the individual attenuation components for different combinations of viscoelastic properties and incident wave frequencies were quantitatively determined, as shown in Fig.4-5.

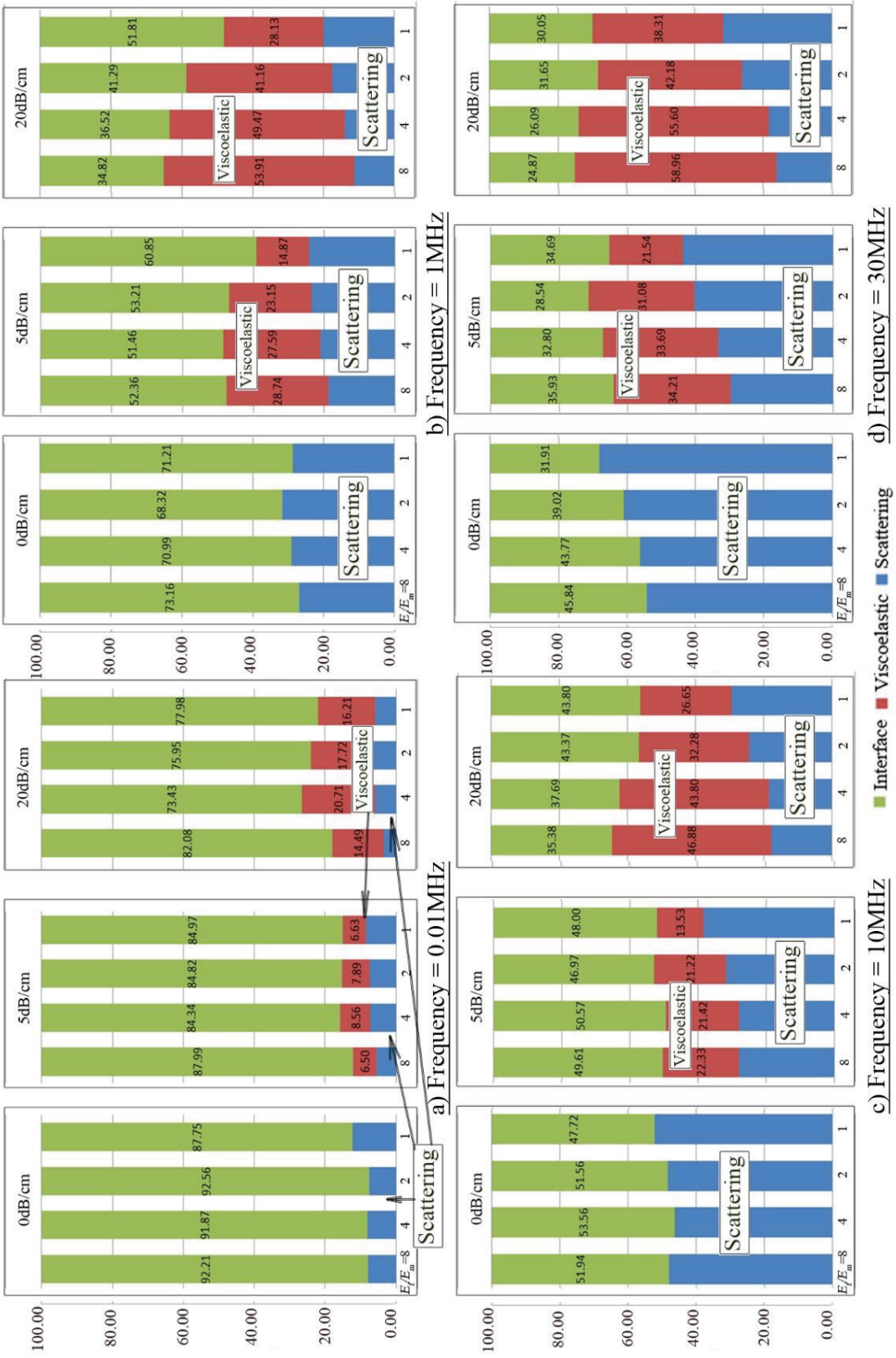

Fig.4-5 Proportions of each attenuation component.

A higher proportion of a particular component means a greater contribution to the dissipation of ultrasonic wave energy. When the matrix viscoelastic attenuation coefficient was 0 dB/cm, the overall attenuation was a combination of energy loss at the interface and scattering attenuation due to the defect. And the energy loss at interface became a major part in the overall attenuation when the incident wave frequency was low, as shown in Figs.4-5(a) and (b). With the increase of incident wave frequency, the proportion of scattering attenuation became larger, due to the gradually obvious scattering waves.

When the matrix viscosity was 5 dB/cm, with the increase of the incident wave frequency, the proportion of viscoelastic attenuation and scattering attenuation became larger. However, due to the weak viscosity of matrix region, the contribution of viscoelastic attenuation was small then the other two attenuation components. When the f was 30 MHz, the main contribution to the overall attenuation was α^{DEF}. And with the E_f/E_m increased from 1 to 8, although both the viscoelastic attenuation and energy dissipation at the interface increased with increasing anisotropy (Figs.4-4(a) and (c)), due to the relative larger increment of α^{VIS}, the proportion of α^{DEF} decreased with increasing E_f/E_m.

When the matrix viscosity was 20 dB/cm, the increment of the viscoelastic

attenuation with incident wave frequency becomes significant. From Figs. 4-5(a) and (d), when E_f/E_m=1, the proportion of α^{VIS} increased by nearly 2.4 times with f increased from 1 to 30 Mhz, while it increased 4 times when E_f/E_m=8. From the above results, the contribution of each individual attenuation components to the overall ultrasonic attenuation under different material viscoelasticity and anisotropy was clarified.

4.4 Conclusion

For a two-layered fiber/matrix composite with transverse defects, the individual acoustic attenuation components (attenuation caused by the viscoelastic nature of the matrix, scattering attenuation caused by transverse defects, and energy loss at the interface) were extracted from the overall attenuation using a newly proposed method. Then, by quantitatively investigating the variation of the individual attenuation components under different combination of the matrix viscosity, material anisotropy and incident wave frequency, the detailed effects of the above factors on the ultrasonic attenuation characteristics were clarified. From the results, the ultrasonic wave attenuation during the propagation in layered composite material is mainly due to the material viscosity and the interface interactions, and all attenuation components represent frequency dependence. At low frequencies, energy dissipation at the interface was the main contribution to the overall attenuation, then the material viscoelastic properties. At

high frequency, the effect of the material viscosity on the overall attenuation became more significant. Through the present analysis, we can quantitatively evaluate the detailed correlation between the various effect factors and the individual ultrasonic attenuation components, especially the frequency characteristics. This ultrasonic wave propagation analysis is promising for the high-precision damage detection technology for composite material with various interfacial imperfections, and the results obtained from our study can provide strong guidance.

References

1. A.I. Beltzer, N. Brauner, Mech. Mater., 6 (1987) 337..

2. A.A. Karabutov, N.B. Podymova, Composites Part B, 56 (2014) 238.

3. L. Zhanli, O. Jay, B. Ted, Wave Motion, 50 (2013) 389.

4. D. Shu, H. Fan, Composites Part B, 27 (1996) 79.

5. J.M. Hale, J.N. Ashton, NDT Int. 21 (1988) 321.

6. E.S. Folias, Int. J. Solids Struct., 25 (1989) 1193.

7. J. Dundurs, J. Compos. Mater.,.12 (2010) 253.

8. S. Biwa, Mech. Mater., 33 (2001) 635.

9. S. Itou, Eng. Fract. Mech., 25 (1986) 475.

10. J. Qu, Int. J. Solids Struct., 31 (1994) 329.

11. S.K. Seth, S. Mark, J.A. Mauro, E.S.C. Carlos, S. Constantinos, Composites Part B, 33 (2002) 87.

Chapter 5

U-DMA Measurement and Dynamic Analysis of Ultrasonic Wave Propagation in Particulate Composites

Chapter 5: U-DMA Measurement and Dynamic Analysis of Ultrasonic Wave Propagation in Particulate Composites

5.1 Introduction

Particle reinforced polymer composite materials have been widely used in various fields due to their excellent properties, of which the main characteristic is viscoelasticity [1]. Dynamic mechanical analysis (DMA) is a general evaluation method for studying the viscoelastic behaviors of polymers, yet it is limited in the low frequency (10^1-10^2 Hz). Ultrasonic Testing technology, due to its sensitivity and accuracy from high frequency, has become one of the several commonly used nondestructive examination technique for material characterization and damage detection [2]. On the basis of previous researches from our group [3-4], we developed a new material evaluation method, Ultrasonic Dynamic Mechanical Analysis (U-DMA), which can be applied into the directly measurement of viscoelasticity at high frequency domain. However, in practical experiments, the measurements are tightly corresponding to various factors, such as matrix viscoelastic properties, particles and defects, incident wave characteristics, and even interfacial bonding condition between particle and matrix. Thus, the mechanisms of wave propagation and its detailed correlation between matrix viscoelasticity, scattering waves due to distributed particles and so on, are still not clear, which may limit to the

actual use of this new evaluation method.

The ultrasonic wave propagation and attenuation characteristics in particulate composite materials can be divided into the part refer to the matrix viscosity and parts affected by the internal particles scattering [5]. For verifying the U-DMA methods and clarifying the detailed influence mechanism of distributed particles, it is necessary to extract and separately investigate the multi-reflected and scattered waves and the corresponding attenuation components. Various studies have been carried out on the independent wave scattering due to particles or defects. For theoretical analysis of wave propagation in particulate composites, Datta [6-8] carried out his works in the problem of plane longitudinal and shear wave propagation in the particulate composite including randomly distribution spherical inclusions, and investigated the correlation between inclusion content, phase velocity and attenuation characteristics of the ultrasonic elastic waves. Beltzer [9] proposed a method consisted the calculation of energy losses due to scattering as well as the viscoelastic losses, by means of a dynamic differential scheme for ultrasonic wave propagation in random particulate viscoelastic composites. Kinra [10], on the other hand, experimentally investigated the propagation of ultrasonic elastic waves in composite material consisting of spherical inclusions distributed randomly in an epoxy matrix. For ultrasonic wave propagation in porous media, Sayers et al. [11] and

Williams et al. [12] studied the scattering waves due to voids in an isotropic media to clarify the effects of the multi-scattering waves on the attenuation characteristics and material mechanical properties. Based on the classic scattering theory, Biwa [13–15] established a theoretical model of viscoelastic composite material for investigating the scattering and absorption attenuation in the particulate composites, by calculating the scattering and absorption cross-section of voids. With consideration of the effects of particle size and radius ratio, and the porosity of the particulate composites, Mylavarapu et al. [16] developed a model for computing the ultrasonic attenuation coefficient, especially the attenuation due to scattering by particles and absorption in epoxy matrix.

In most of aforementioned works, the interactions between neighboring particles are neglected, and the effects of these fillers on wave propagation behavior and attenuation characteristics are only related to the independent scattering, which is in terms of the dimension and content. Thus, there are still no well-defined models or solutions, which can accurately explain the influences of particles. On the basis of the method developed in previous chapters, which can separately investigate the individual wave components and attenuation components, we emphasize on the analysis about the multi-reflection and scattering waves, especially the mutual interactions among distributed particles.

The dynamic mechanical properties of actual particulate composites samples are

firstly characterized by U-DMA measurement. Based on the data and by using the time-domain finite element analysis for ultrasonic wave propagation, 2-D FEM models for particle reinforced composite materials with different particle content are built. The influences of particles on wave propagation characteristics can be extracted and systematically investigated. The ultrasonic wave attenuation characteristics due to multi-reflection and scattering waves from particles are emphasized and systematically discussed. Reasonable results are obtained by comparing the ultrasonic wave attenuation coefficients and viscoelastic properties, and the validity for both U-DMA measurement and FEM simulation results are verified.

5.2 Sample Characterization and FEM Model Establishment

5.2.1 Sample Preparation

In this chapter, two kind of particle reinforced composite materials are synthesized by room temperature vulcanizing silicone rubber and, TiO_2 and ZnO particles respectively, which may be applied to the acoustic lens in medical ultrasonic testing. The RTV silicone rubber used here is two-component type, KE106, which is produced by Shin-Etsu Chemical Co., Ltd. And the TiO_2 and ZnO particles, which have average size of 5μm and 50nm respectively, are produced from Wako Pure Chemical Industries, Ltd.

Samples with different weight fraction of TiO_2 and ZnO particles are prepared. With

the weight fraction of both two kind of particles from 10 to 20 wt%. For comparison, the pure silicone rubber samples are also prepared.

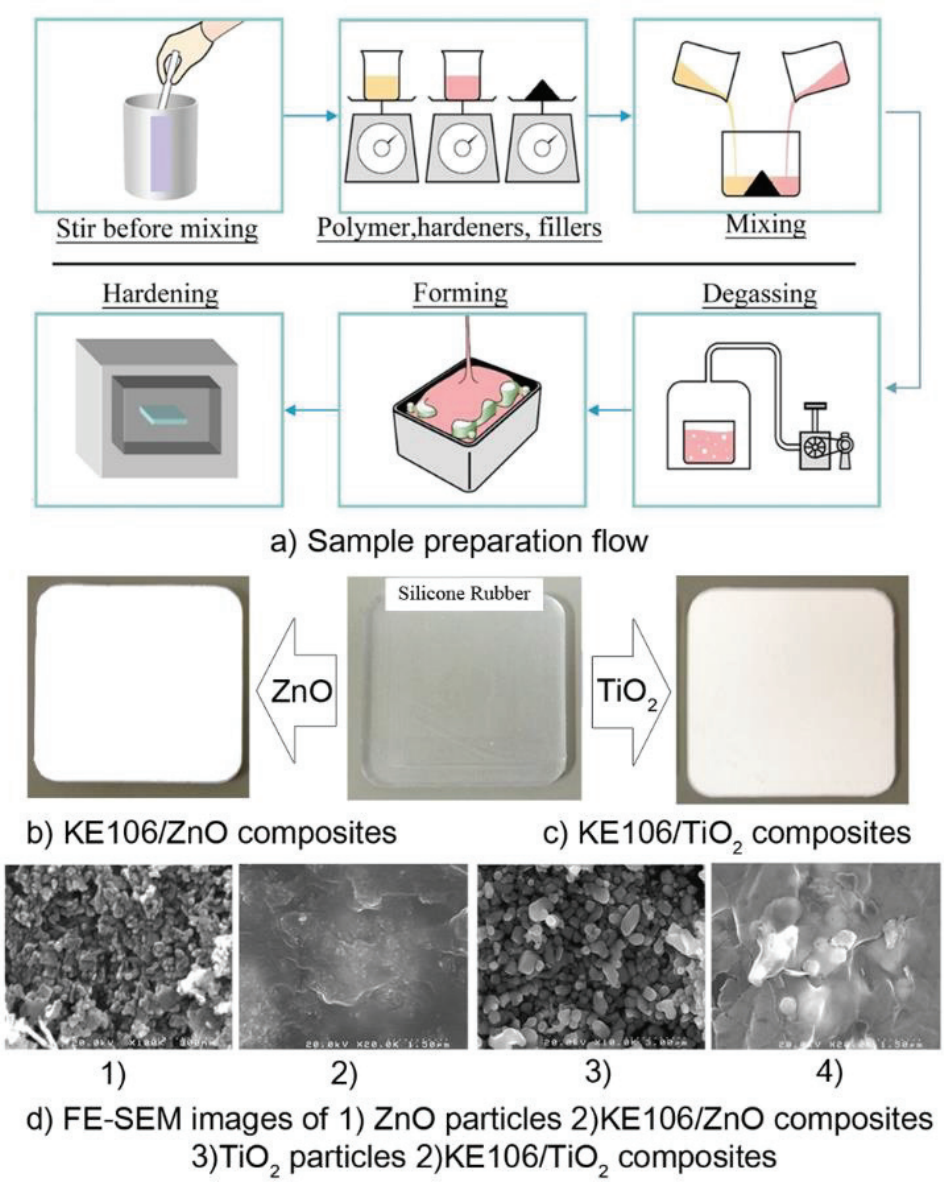

Fig.5-1 Sample preparation of particulate composite material and FE-SEM characterization.

The sample preparation procedure is depicted in Fig.5-1(a) [17]. In the process of mixing, the added particles are dispersed by using ultrasonic homogenizer [18]. From the

Field Emission-Scanning Electron Microscope (FE-SEM) figures in Fig.5-1(d), most of the TiO_2 particles are effectively dispersed in the rubber. For ZnO particles, although the particles are well dispersed into the matrix, slight agglomeration can also be detected. The particles are with mostly circular in shape, and the size of TiO_2 particles can be seen varied from 3.5 to 5.5 μm, while that of ZnO particles varied from 20 to 50 nm. Then, density test, tensile test, and dynamic mechanical analysis were carried out [17, 19].

5.2.2 U-DMA Method

Herein, ultrasonic wave propagation characteristics are utilized in the dynamic mechanical analysis. We have already known that, for two-dimensional time-harmonic stress waves in an isotropic media, the ultrasonic wave equations are [20]:

$$\left.\begin{aligned}\left(\mathrm{K}+\frac{4}{3}\mathrm{G}\right)\frac{\partial^2 u_x}{\partial x^2}+\left(\eta_\mathrm{v}+\frac{4}{3}\eta_\mathrm{s}\right)\frac{\partial^3 u_x}{\partial t\,\partial x^2}&=\rho\frac{\partial^2 u_x}{\partial t^2}\\ \mathrm{G}\frac{\partial^2 u_y}{\partial x^2}+\eta_\mathrm{s}\frac{\partial^3 u_y}{\partial t\,\partial x^2}&=\rho\frac{\partial^2 u_y}{\partial t^2}\end{aligned}\right\} \tag{1}$$

the first term on the left-hand denotes the elastic component, in which K is the bulk modulus, and G is the shear modulus; the second term indicates the viscous component, in which η_v is for the bulk viscosity, and η_s is the shear viscosity coefficient, ρ is density. For general wave equation, the displacement can be expressed as: $u = Ae^{i(\kappa x-\omega t)}$. By introducing the complex elastic modulus, $E^* = E' + iE''$, where E' is for the elastic component and the E'' is for the viscous component, Eq.(1) can be rewritten as:

$$\rho \frac{\partial^2 u_x}{\partial t^2} = E' \frac{\partial^2 u_x}{\partial x^2} + \eta \frac{\partial^3 u_x}{\partial t \partial x^2} = (E' + i\omega\eta) \frac{\partial^2 u_x}{\partial x^2} = E^* \frac{\partial^2 u_x}{\partial x^2} \tag{2}$$

where $i\omega\eta$ denotes the viscous component. By using the complex velocity, c^*, the complex modulus can be expressed as:

$$E^* = \rho(c^*)^2 \tag{3}$$

From the sound dispersion, we know that:

$$\frac{1}{c^*} = \frac{1}{c} - i\frac{\alpha}{\omega} \tag{4}$$

then,

$$c^* = c' + ic'' = \frac{c}{1+(\frac{\alpha c}{\omega})^2} + i\frac{\alpha c^2}{\omega} \cdot \frac{1}{1+(\frac{\alpha c}{\omega})^2} \tag{5}$$

thus, the complex elastic modulus, E^*, can be expressed as:

$$E^* = E' + iE'' = \rho(c^*)^2 = \rho c^2 \frac{1-(\frac{\alpha c}{\omega})^2}{\left\{1+(\frac{\alpha c}{\omega})^2\right\}^2} + i\rho c^2 \cdot \frac{2\frac{\alpha c}{\omega}}{\left\{1+(\frac{\alpha c}{\omega})^2\right\}^2} \tag{6}$$

In Eq.(6), the first term is the storage modulus, *E'*, the second term is for the loss modulus, *E"*, and α is the ultrasonic attenuation coefficient, ω is for the angular frequency. Then, the loss tangent, *tan δ* can be derived by the following:

$$tan\,\delta = \frac{2\frac{\alpha c}{\omega}}{1-(\frac{\alpha c}{\omega})^2} \tag{7}$$

Herein, the oscillating energy generated by the ultrasonic wave at the left and right edge (see Fig.5-2), I_{in} and I_{out}, were utilized to calculate the ultrasonic attenuation coefficient [21]:

$$\alpha(f) = \frac{1}{L}\ln\left(\frac{I_{in}}{I_{out}}\right) \tag{8}$$

L is the wave propagation length. In the case of a plane advancing wave, the following formula is used to calculate the oscillating energy, where c is wave velocity [21]:

$$I = \frac{P^2}{\rho c} \tag{9}$$

Therefore, from the viewpoint of ultrasonic wave propagation, the elastic and viscous component of viscoelastic property can be characterized by evaluating the wave characteristics, such as attenuation coefficients, phase velocity. By utilizing the previously developed ultrasonic viscoelastic measurement device [3,4], U-DMA measurement is carried out on the basis of bottom reflection method.

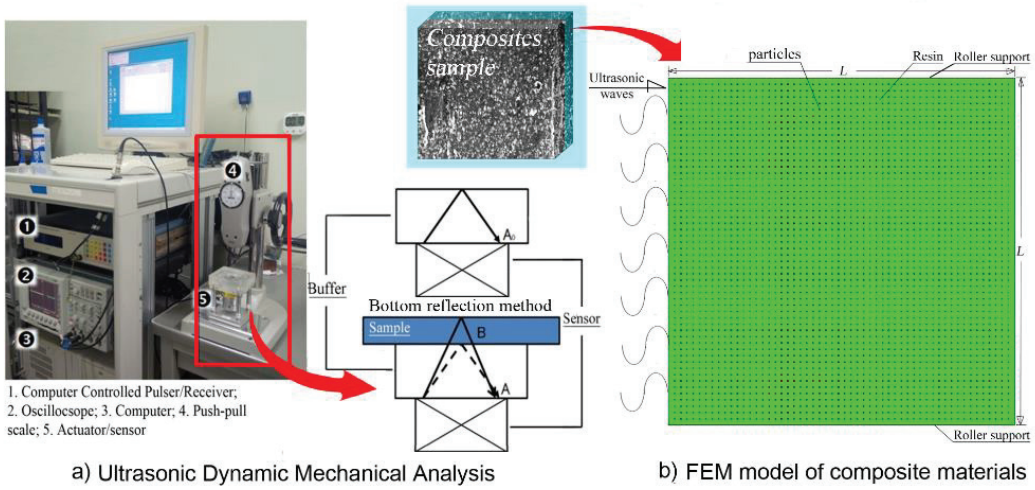

Fig.5-2 a) Dynamic mechanical characterization by using Ultrasonic wave;b) 2-D FEM modelling.

Fig.5-2(a) depicts the measurement device and schematic. The transducer is both

pulser and receiver, with its total band of 0.5 to 30 MHz, and bonded with the buffer layer and composites sample by couplant. The ultrasonic signals with sinusoidal waveform are incident from the transducer to the sample through buffer layer. Then, the echoes from buffer/air interface (A_0 signals), buffer/sample interface (A signal), and the echoes from bottom interface (B signals), are processed by fast Fourier transform (FFT) transform for obtaining the frequency spectrums of wave signals. Then, the attenuation coefficient and phase velocity are calculated by following equations:

$$\alpha(f) = \frac{1}{2h} ln(\frac{A_0(f)^2 - A(f)^2}{A_0(f)B(f)}) \tag{10}$$

where $A_0(f)$, $A(f)$, $B(f)$ are the absolute value of spectrum of aforementioned three echoes at the corresponding wave frequency, *f*. *h* is the thickness of sample. From the processed real part and imaginary part of echoes *A(f)* and *B(f)*, the phase velocity can be obtained by:

$$V_P(f) = \frac{2h\varpi}{tan^{-1}\frac{Im[B(f)]}{Re[B(f)]} - tan^{-1}\frac{In[A(f)]}{Re[A(f)]} + 2N\pi + \varpi T} \tag{11}$$

where ω is the angular frequency, *T* is the time domain after multiplying the window function during FFT transform, $2N\pi$ is the phase correction constant when calculating the arc tangent. The resulting ultrasonic wave attenuation coefficient and phase velocity are then applied to calculation of storage modulus and loss modulus, according Eq.(6).

5.2.3 FEM Analysis

Based on the U-DMA results, 2-D FEM models are established, which represent for the cross-section of sample. It is already known that, the particles in matrix usually show random distribution pattern, and various shapes and dimensions. Therefore, before the establishment of particulate composite materials, the following assumptions are made so that the variables can be reduced: 1) there are not any overlapping regions between particles; 2) the particles are all in the same dimension and circular shape; 3) the particles are periodic distributed in the matrix [22]; 4) The particles and matrix are perfectly bonded. When the particle content increased, the surface density increased with the quantity of particles. Herein, the geometry of the 2-D FEM models used here is 1mm*1mm, and the diameter of TiO_2 particles is assigned to 5 μm. For ZnO particles, with consideration of the slight agglomeration, the diameter is set to 500nm. The established particulate composite material models are depicted in Fig.5-2(b), in which the region colored in green is silicone rubber, and the black circles represent the particles. Absorbing boundary condition is assumed on the right side where no reflection wave will occurs, and the upper and lower edges are set to be roller supports.

Both of the particles and matrix in the model are considered as homogeneous and isotropic materials. The distributed particles are assigned to be elastic material, while the

matrix is of viscoelastic properties [20]. Based on our previous works [21], the matrix and the added particles are distinguished by specifying the density, longitudinal and transverse wave velocity, rather than specifying the elastic modulus of individual region. From the viscous component which is indicated in Eq.(6), by introducing the viscoelastic attenuation into matrix region and specifying the attenuation coefficient, the viscosity can be determined. Here, for both TiO_2 and ZnO particles, the particle content is assigned to be varied from 10 to 20 wt%, as same as the prepared actual samples. The time-harmonic longitudinal stress wave loadings in single frequency are applied vertically to the left edge of the model [22], as shown in Fig.5-2(b), which has one-cycle sinusoidal waveform with its amplitude of 1 MPa. The applied incident wave frequency in FEM analysis is assigned to be varied from 1 to 32 MHz, as same as the total band of transducer in U-DMA measurement.

5.3 Results of U-DMA Measurement

Through U-DMA measurement, the dynamic mechanical properties for the prepared TiO_2/KE106 and ZnO/KE106 particulate composites samples are carried out, from which we obtained the ultrasonic attenuation coefficient, storage and loss modulus, and the loss tangent in the frequency domain of 1 to 5 MHz (the effective frequency of U-DMA device), as depicted in Figs.5-3 and 5-4.

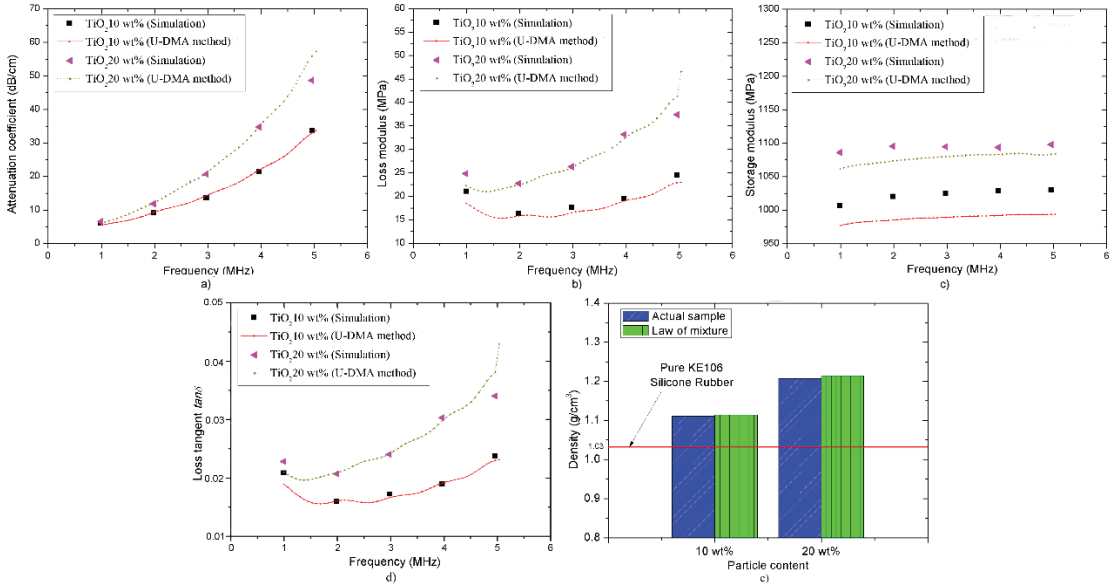

Fig.5-3 FEM model validation for TiO_2/KE106 composite materials: a) Attenuation coefficient; b) Loss modulus; c) Storage modulus; d) Density from actual sample and Law of mixture.

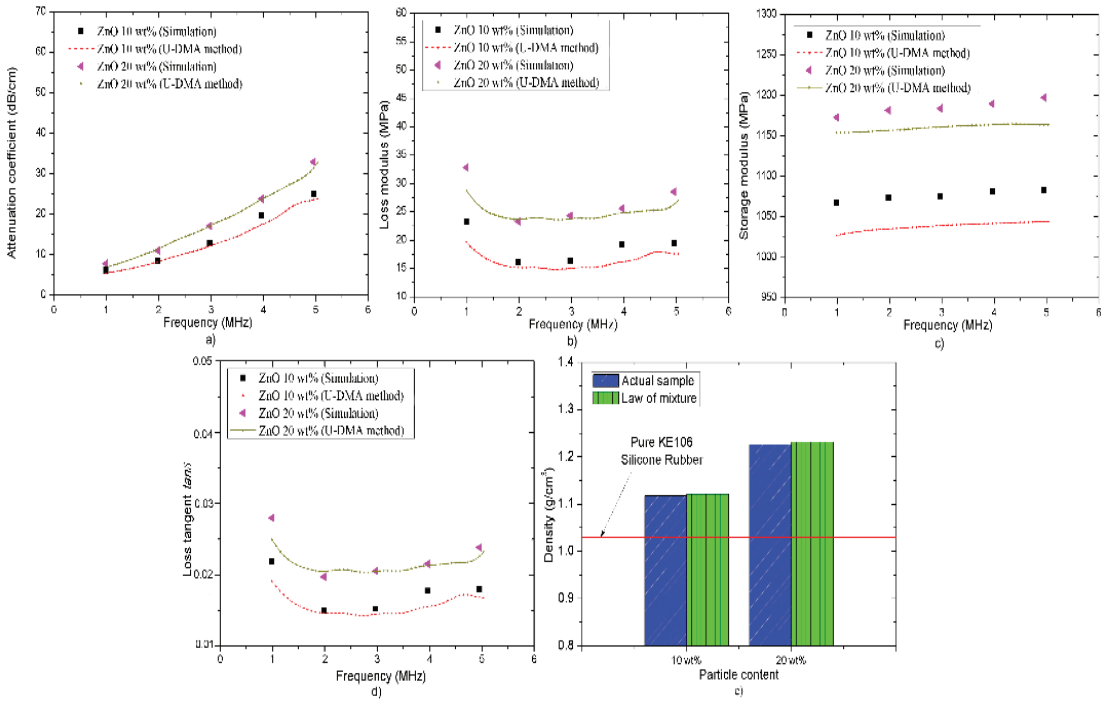

Fig.5-4 FEM model validation for ZnO/KE106 composite materials: a) Attenuation coefficient; b) Loss modulus; c) Storage modulus; d) Density from actual sample and Law of mixture.

Although the introduction of particles provide enhanced density and elastic properties, the variation of attenuation coefficient and loss modulus with incident wave frequency are more obvious, which result in the increment of loss tangent, tan δ. In particular when the incident frequency is over 2 MHz, the loss tangent of the TiO_2/KE106 particulate composites is improved by 82%, while in ZnO/KE106 composites the maximum increment becomes 15%. From the ultrasonic wave propagation simulation, the dynamic mechanical properties are also evaluated, and the results are also depicted in Figs.5-3 and 5-4. It can be seen that, the results of attenuation coefficient, loss modulus and loss tangent from simulations present good agreement with U-DMA results.

In the actual particulate composite material sample preparation, the degassing process cannot completely remove the internal air bubbles, which results in the relative lower value of density in actual sample than that from Law of mixture, as shown in Figs.5-3(e) and 5-4(e). The air bubbles can also reduce the ultrasonic wave phase velocity by means of causing scattering waves among particles and bubbles. From the elastic component in Eq.(6), the reduction of density and phase velocity leads the storage modulus to decline accordingly. Therefore, as shown in Fig.5-3(c) and 5-4(c), the storage modulus of actual samples from U-DMA is lower than that in simulation. When the particle content increases from 10 to 20 wt%, more air bubbles were introduced into the

samples, which leads to the increment of density difference between actual samples and law of mixture. However, as depicted in Figs.5-3(a) and 5-4(a), the more air bubbles in the case of particle content of 20 wt% don't produce more difference of ultrasonic wave attenuation between actual samples and simulation results. Instead, for composites with relative lower particle content, the difference of loss modulus between actual sample and simulation is more obvious. From the viscous component in Eq.(6), it is clear that, when particle content is 10 wt%, the reduction of wave phase velocity due to air bubbles is greater than that of 20 wt%, which results that the difference between actual experiments and simulation became smaller with the increasing of particle content. Thus, it is clear that, the difference of elastic modulus is due to the introduced air bubbles, and the results from both U-DMA and FEM simulation are reasonable.

5.4 FEM Analysis and Discussion

Then, for the influence mechanism of particles, we systematically investigate the multi-reflection and scattering waves, and the corresponding attenuation characteristics, based on the established TiO_2/KE106 and ZnO/KE106 composite models.

5.4.1 Ultrasonic Propagation Behaviors in Micro-size TiO_2 Particle Reinforced Composites

In order to make the influences of micro-size particles on ultrasonic propagation

more clear to discuss, the ultrasonic wave propagation behaviors in the region of a quarter of the whole FEM model are presented. Figs.5-5(a) and (b) depict the ultrasonic propagation patterns in pure silicone rubber and particulate composites, respectively. Due to the direct correspondence between waveforms and dynamic stress, the propagation pattern in Fig.5-5 can also represent the internal stress distribution.

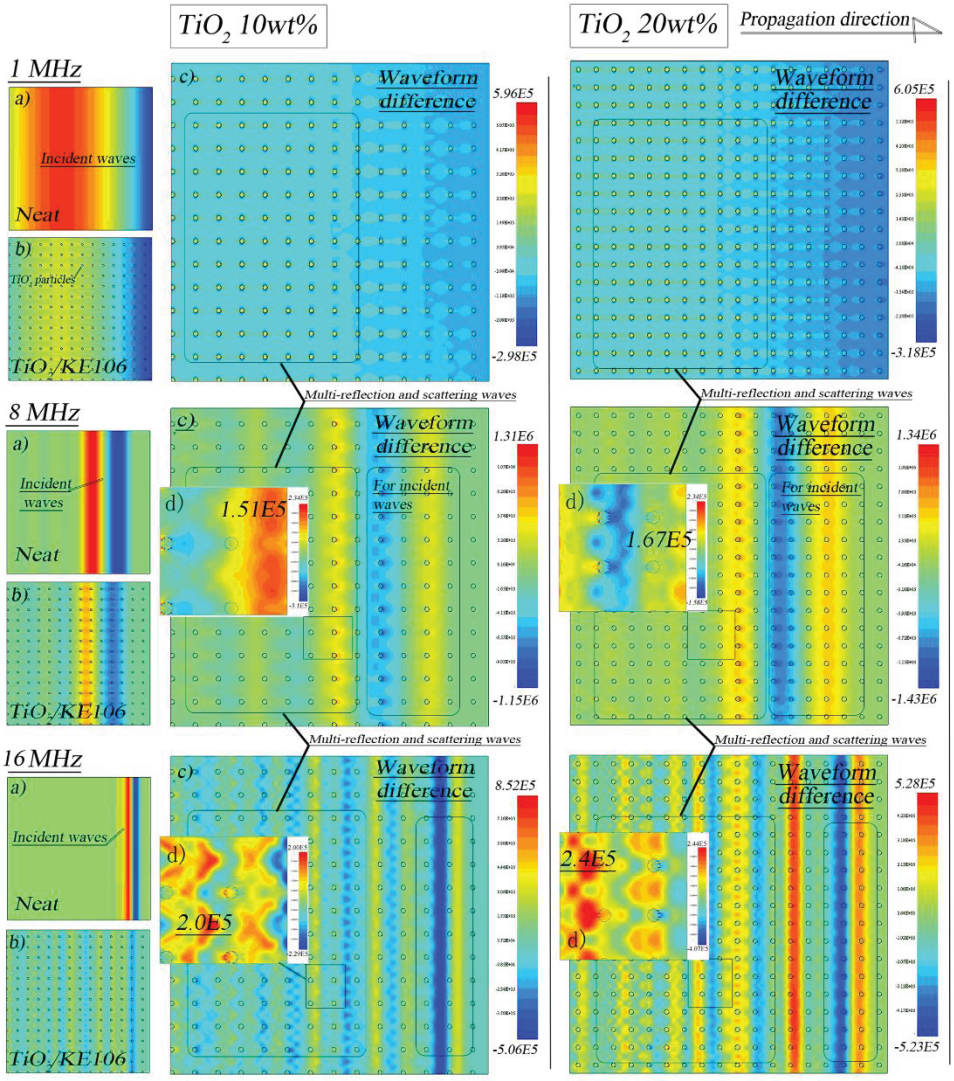

Fig.5-5 Ultrasonic propagation behavior: a) pure silicone rubber; b) TiO_2/KE106 composite materials; c) extracted waveform difference.

In the figures, the deep blue region means that the region is under compression, while the deep red region means tension. With the increment of incident wave frequency, the region with deep blue and red narrows down with the decrement of wave length. When the particles are introduced into the composite, multi-reflection and scattering waves occurred among the particles during the waveform propagation, as depicted in Fig.5-5(b). By extracting the waveform difference, as shown in Fig.5-5(c), the dissipated incident waves, and the multi-reflection and scattering waves, can be separately discussed. In Fig.5-5(c), the region with relative deeper color near the right edge denoted the dissipated incident waves. The deeper color of this region means more incident waves are dissipated. The waveforms in the left region behind the incident waves are for multi-reflection and scattering waves.

When incident wave frequency is 1 MHz, due to the relative larger wave length comparing to the particle dimension, no apparent multi-reflection and scattering waves can be seen. And with the particle content increased from 10 to 20 wt.%, the maximum value of the color scale only increased from 0.6 to 0.61 MPa. With the incident wave increased to 8 MHz, due to the diminishing of wave length, the influence of particle on ultrasonic wave propagation become remarkable. From the closeup view during the region for multi-reflection and scattering waves, as shown in Fig.5-5(d), as the particle

content increased, the maximum stress value increase from 0.15 to 0.17 Mpa, which means the interactions among particles become greater. Thus, although the increment of particle quantity reduced the matrix viscosity, since more incident waves are reflected and scattered during the wave propagation, the difference between neat rubber and particulate composites grow with the increment of particle content. When the incident wave frequency reached 16 MHz, since the wave length gets closer to the particle dimension, the interactions among particles become more significant, and the region containing multi-reflection and scattering waves become larger obviously. With the incident wave frequency increased from 8 to 16 MHz, as depicted in Fig.5-5(d), the maximum stress value increased almost 0.05 MPa. This results in that more incident waves are dissipated during the propagation, and lead to the decrement of stress value in the region represent for the dissipated incident waves.

5.4.2 Ultrasonic Propagation Behaviors in Nano-size ZnO Particle Reinforced Composites

Since the ZnO particle is in nano scale, we present the ultrasonic wave propagation behaviors in the region of one-sixteen of the whole FEM model, as depicted in Fig.5-6. As same as the above section, Fig.5-6(c) represents the waveform difference between neat rubber (Fig.5-6(a)) and ZnO/KE106 composite materials (Fig.5-6(b)). When the incident

wave frequency is at the range of 1 to 8 MHz, due to the small dimension of ZnO particles, no apparent multi-reflection and scattering waves can be detected.

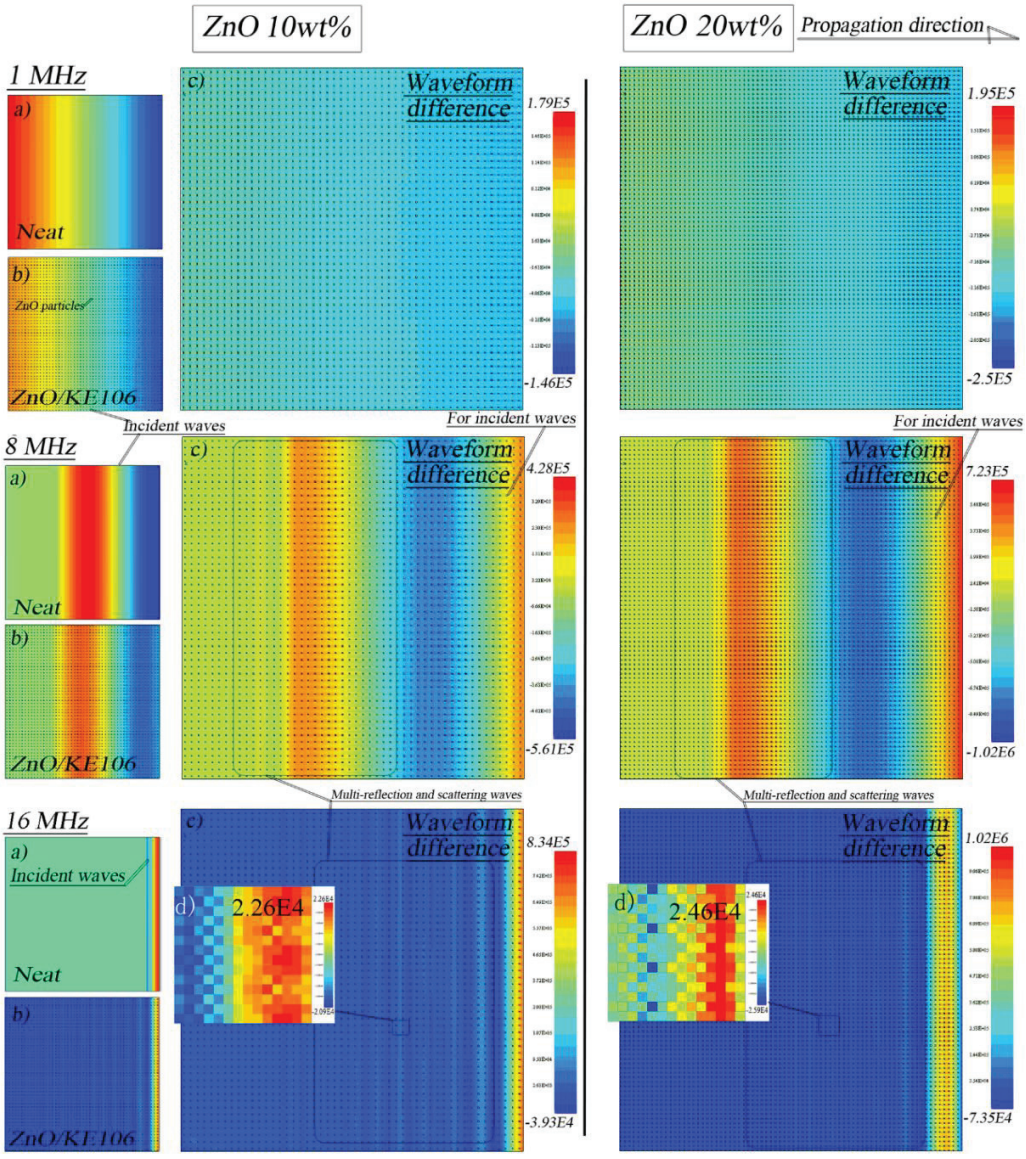

Fig.5-6 Ultrasonic propagation behavior: a) pure silicone rubber; b) ZnO/KE106 composite materials; c) extracted waveform difference.

For instance, when the incident wave is 8 MHz and the particle content is 20 wt%,

the maximum value of color scale for ZnO/KE106 composite material is of 0.6 MPa smaller than that in TiO_2/KE106 composite materials. At 16 MHz, the interactions among particles can be detected at the region behind the incident waves. However, with comparison to the case of TiO_2 particulate composites, the maximum stress value of reflection and scattering waves is much lower. As shown in Fig.5-6(d), with the particle content increase from 10 to 20 wt%, the maximum stress value of multi-reflection and scattering waves only increase 0.002 MPa, which means the interactions among ZnO particles are weaker than that in TiO_2/KE106. Although the ZnO/KE106 has more quantity of particles, the particle dimension has played a decisive role.

Thus, from the dynamic internal stress distribution, the influence of particles on the ultrasonic wave propagation are cleared. The correlation between propagation behaviors, especially the internal multi-reflection and scattering waves, incident wave frequency, particle content and dimension, are clarified.

5.4.3 Investigation of the Individual Attenuation Components

From Beltzer [9] and Biwa [14], the total wave attenuation is the sum of matrix viscosity and the scattering loss from internal inclusions. In classic scattering theory, the wave scattering attenuation component can be estimated based on the single-particle scattering under low frequency limit [14]:

$$\alpha^{SCA} = \frac{1}{2} n_s \gamma^{SCA} \tag{12}$$

where α^{SCA} is for the scattering attenuation component, ns is the number of inclusions, and γ^{SCA} represents for the independent scattering cross-section. However, from the ultrasonic wave propagation analysis in previous sections, the multi-reflection and scattering waves among particles can significantly affect the internal propagation behavior. Thus, for the presented particulate composites model, the total ultrasonic attenuation coefficient αsum is written in the following form:

$$\alpha^{SUM} = (1 - \phi)\alpha^{VIS} + \alpha^{PAR} + \alpha^{INT} \tag{13}$$

where α^{VIS} is for the energy loss in resin matrix, $(1 - \phi)$ means removing the volume of particles (because our model is 2-D, we use here the area percentage of defect area); α^{PAR} denotes the energy loss due to the independent scattering from particles. α^{INT} is the energy dissipation caused by the interactions between particles, which could be significantly changed by the particle content and dimension, and the incident wave frequency. This attenuation component is the key issue for investigating the detailed effect mechanism of particles.

Therefore, the variation behavior of attenuation coefficient (α^{SUM}) against particle content (for both TiO_2 and ZnO particle, 10 to 20 wt.%) and incident wave frequency (1 to 16 MHz) are investigated, the results are depicted in Fig.5-7. For comparison, the

attenuation coefficient of pure silicone rubber model ($\alpha^{SUM} = \alpha^{VIS}$) are also presented in Fig.5-7, which are represented as black bar in twill lines.

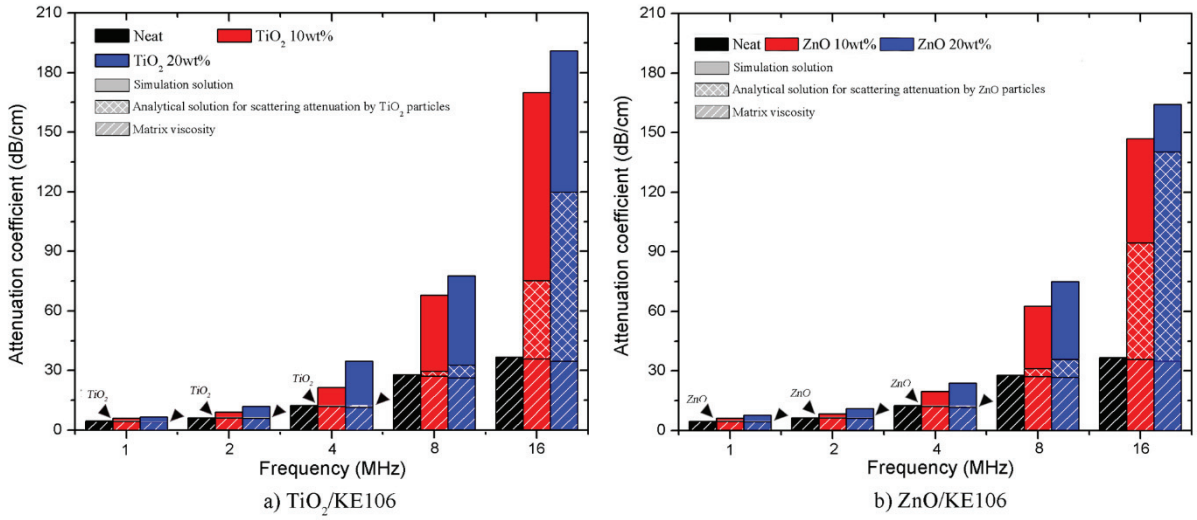

Fig.5-7 Variation behavior of attenuation coefficient with incident wave frequency and particle content for TiO_2/KE106 and ZnO/KE106 composite materials.

It can be seen that, with the incident wave frequency increased from 1 to 16 MHz, due to the frequency dependence of matrix viscosity, the attenuation coefficient of neat rubber grows, and reached its maximum value of 36.8 dB/cm at 16 MHz.

The other bars in Figs.5-7(a) and (b) represented the overall attenuation coefficient of TiO_2/KE106 and ZnO/KE106 composites models with different particle content, in which the part with twill lines represents for the matrix viscosity, $(1-\phi)\alpha^{VIS}$. The rest part containing grid part and no lines part represents the attenuation component due to internal particles, $\alpha^{PAR}+\alpha^{INT}$. It can be seen that, in both TiO_2/KE106 and ZnO/KE106

composites models, the overall attenuation coefficients increase with the incident wave frequency. Comparing to the variation of matrix viscosity, the contribution of energy loss due to particles to the overall attenuation grow significantly. When the incident wave frequency is below 4 MHz, due to the weak interactions among particles, the main part in overall attenuation is matrix viscosity; while the incident wave frequency is over 8 MHz, the part of $\alpha^{PAR}+\alpha^{INT}$ provide the major contribution. And with the particle content increased from 10 to 20 wt.%, although the matrix viscosity slight decreased, due to more incident waves are reflected and scattered by particles, the contribution of particles get larger, and lead to the increment of overall attenuation coefficient with particle content.

Although the ZnO/KE106 composites models have more quantity of particle, the relative small particle dimension results in the relative weaker interactions among particles. At the range of 1 to 2 MHz, because the main part of the overall attenuation is matrix viscosity, the attenuation coefficient for these two composite materials are at the same level. When the incident wave frequency increased from 2 MHz, the multi-reflection and scattering in TiO_2/KE106 composites models become greater than that in ZnO/KE106 composites models. As shown in Fig.5-7, the part of αpar+αint for TiO_2/KE106 composites models become obvious larger than that in ZnO/KE106 composites models. For instance, when the particle content is 20 wt% and incident wave

frequency is 16 MHz, the part of $\alpha^{PAR}+\alpha^{INT}$ for TiO_2/KE106 composites model is of 27 dB/cm larger than that in ZnO/KE106 composites model.

5.4.4 Interactions among Particles

For investigating the detailed effects of interactions between particles, the independent wave scattering attention is calculated based on the classical scattering theory, as denoted in Eq.(12). The scattering cross-section of inclusions can have the following expressions [14]:

$$\frac{\gamma^{sca}}{a^2} = \frac{4\pi}{9} g_c \left(\frac{2\pi f a}{c_{L1}}\right)^4 \tag{14}$$

where the coefficient g_c is a constant related to the material properties [25]:

$$g_c = \left(\frac{K_1 - K_2}{K_2 + \frac{4}{3}\mu_1}\right)^2 + \frac{1}{3}\left[1 + 2\left(\frac{\kappa_1}{K_1}\right)^3\right]\left(\frac{\rho_2}{\rho_1} - 1\right)^2 + \frac{2}{5}\left[2 + 3\left(\frac{\kappa_1}{K_1}\right)^5\right]\left[\frac{10(\mu_1 - \mu_2)}{4(\mu_2 - \mu_1) + (6\mu_2 + 9\mu_1)\left(\frac{\kappa_1}{K_1}\right)^2}\right]^2 \tag{15}$$

the subscript *1* and *2* are for matrix and inclusion, respectively. K is the bulk modulus, and μ is the lame constants. K and κ represented for wave numbers for compressional and shear waves. The calculated results are depicted in Fig.5-7, the region in bars marked as grid denoted the calculated scattering attenuation due to TiO_2 and ZnO particles, respectively.

From Eq.(14), the scattering attenuation was proportional to the 4th power of the incident wave frequency, and led to the extreme small of α^{PAR} at the range of 1 to 4 MHz.

At this range, the major part of $\alpha^{PAR}+\alpha^{INT}$ is the energy loss due to interactions among particles, α^{INT}. When incident wave frequency increased from 8 MHz, as depicted in Figs.5-7(a) and (b), α^{INT} significantly reduced with the increase of the independent scattering attenuation of particles. Because the particle quantity in ZnO/KE106 composites model is much larger, from the calculation of independent scattering in Eq.(12), the α^{INT} for ZnO particles increase more significantly than that in TiO_2/KE106 composites model.

Thus, from the ultrasonic attenuation characteristics of TiO_2 and ZnO particle reinforced composite materials, when the wave length of incident wave gets closer to the particle dimension, the energy dissipation due to the multi-reflection and scattering is the major part in overall attenuation. And it is also clear that, the particle dimension and quantity can significantly change the ultrasonic attenuation characteristics by means of affecting the ultrasonic propagation behavior.

Therefore, it can be summarized that, by means of affect the wave propagation and attenuation characteristics, the interactions among particles can significantly affect the material viscoelastic properties.

5.5 Conclusion

Ultrasonic Dynamic mechanical analysis (U-DMA), as a new ultrasonic testing

technology for material characterization, has been applied to the viscoelasticity evaluation of particle reinforced polymer composites with different type and content of particles. Reasonable results of ultrasonic wave attenuation and viscoelastic characteristics are obtained by comparing with the result from time-domain finite element analysis for ultrasonic propagation in particulate composite materials. The multi-reflection and scattering waves due to particles, and the corresponding attenuation components, are emphasized and discussed with consideration of the mutual interactions among particles. By extracting and separately investigating the multi-reflection and scattering waves, it is clear that the interactions among particles are playing a major role in the ultrasonic propagation and dynamic internal stress distribution. From the variation behavior of attenuation coefficient and viscoelasticity against particle weight fraction and incident wave frequency, the detailed influence mechanism of interactions among particles on both ultrasonic attenuation and viscoelastic characteristics are also clarified. Therefore, the newly developed Ultrasonic Dynamic Mechanical Analysis (U-DMA) method and the finite element analysis method for ultrasonic propagation in particulate composites are both proved to be reasonable and feasible in actual characterization of composite materials, and will provide strong guidance for further development of high precision ultrasonic technologies in particulate composite materials.

References

1. R.A. Malloy, J.A. Hudson, Int. encycl. Compos., VCH (1990).

2. P. Mix, Introduction to nondestructive testing-a training guide. New York (1987).

3. N. Omada, T. Suha, H. Furusawa, S. Urabe, T. Kondo, Q.Q. Ni, Ultrasonics, 44 (2006) 211.

4. T. Kunizawa, T. Kondon, Q.Q. Ni, Trans. J. Soc. Mech. Eng. Ser. A, 73 (2007) 775.

5. H. Krautkramer, J. Krautkramer, Ultrason. Test. Mater., New York, (1969).

6. S.K. Datta, Archives Mech. 28 (1976) 317.

7. S.K. Datta, Continuum model of discrete systems. University of Waterloo Press, (1978) 111.

8. S.K. Datta, H.M. Ledbetter, Y. Shindo, A.H. Shah, Wave motion, 10 (1988) 171.

9. A.I. Beltzer, C.W. Bert, A.G. Striz, Int. J. Solids Struct., 9 (1983) 785.

10. V.K. Kinra, M.S. Petraitis, S.K. Datta, Int. J. Solids Struct., 16 (1980) 301.

11. C.M. Sayers, R.L. Smith, Ultrasonic, 20 (1982) 201.

12. J. H. Williams, Jr. S.S. Lee, H. Yuce, NASA Contractor Report 3693 (1983).

13. S. Biwa, Mech. Mater., 33 (2001) 635.

14. S. Biwa, S. Idekoba, N. Ohno, Mech. Mater., 34 (2002) 671.

15. S. Biwa, Y. Watanabe, S. Motogi, N. Ohno, Ultrasonics. 43 (2004) 5.

16. P. Mylavarapu, E. Woldesenbet, Compos. part B, 41 (2010) 42.

17. I.A. Al-Ajaj, M.M. Abd, H.I. Jaffer, Int. J. Min. Metal. Mech. Eng., 1 (2013) 93.

18 B. Bittmann, F. Haupert, A.K. Schlarb, Ultrason. Sonochem., 18 (2011) 120.

19. A. Chatterjee, M.S. Islam, Mater. Sci. Eng., A, 487 (2008) 574.

20. J.L. Rose. Cambridge University Press. London, 1999, p. 24.

21. J.J. Chang, C.L. Zheng, Q.Q. Ni, Compos. Struct., 1-4 (2006) 451.

22. S.K. Kanaun, V.M. Levin, F.J. Sabina, Wave motion, 40 (2004) 69.

23. J. Zhang, W.J. Ye, Ultrasonics, 62 (2015) 27.

24. A.N. Norris, Int. J. Eng. Sci., 24 (1886) 1271.

Chapter 6

General Conclusions

Chapter 6: General Conclusions

This thesis has systematically investigated the ultrasonic wave propagation behaviors and the corresponding dynamic stress distribution in both fiber- and particle-reinforced composite materials, with consideration of the influence of material viscoelastic properties and anisotropy, bonding condition between constituent phases and interfacial interactions, as well as incident wave frequency.

In chapter 2, for bimaterial composite with ellipse-shaped defect, a new method combining stress distribution evaluation and ultrasonic propagation analysis is established. From this method, the correlation between ultrasonic wave propagation and stress singularities, dynamic stress distribution is investigated. It is clear that the material properties are closely related to the ultrasonic wave propagation. By changing the material property, with E_f/E_m changing from 1 to 8, the free edge effect and wave mode conversion at the interface become more remarkable. Since the resulting scattering waves caused by stress singularity at free edge and wave conversion at the interface, the ultrasonic propagation behavior become more complicated. Using the dynamic waveform analysis during ultrasonic wave propagation, the stress echo from the free edge and interface and the influence of scatting wave are clarified. The stress concentration phenomenon at the defect tips with the influence of free effect and interface stress concentration are evaluated.

The simulation results showed the method using ultrasonic wave propagation analysis is a convenient and effective way to evaluate the interaction between material properties, stress singularities and dynamic internal stress distribution in composite materials.

In chapter 3, based on the 2-D two layered composite materials with ellipse-shapes transverse defect which was established in the previous chapter, we proposed a new method for investigating the detailed influence mechanism of material viscoelastic property and anisotropy on ultrasonic wave propagation and attenuation characteristics, of which the key issue is the extraction of each individual attenuation components, including viscoelastic attenuation, wave scattering attenuation, and the interface interactions. Based on the dynamic internal stress analysis method proposed in chapter 2, the variation of interfacial shear stress distribution with material anisotropy and viscoelasticity are studied and applied in the investigation of influence mechanisms. The results showed that energy dissipation caused by interface interactions is a major part of the overall ultrasonic wave attenuation. Each attenuation component is closely related to the material anisotropy and matrix viscoelastic properties.

In chapter 4, the incident wave frequency is taken into consideration as an important effect factors. On the basis of extraction of each individual attenuation component as proposed in chapter 3, the frequency characteristics of these attenuation components

under various combinations of material viscoelastic and anisotropy properties are quantitatively clarified. And the detailed effects of the above factors on the ultrasonic attenuation characteristics were clarified. From the results, the ultrasonic wave attenuation during the propagation in layered composite material is mainly due to the material viscosity and the interface interactions, and all attenuation components represent frequency dependence. At low frequencies, energy dissipation at the interface was the main contribution to the overall attenuation, then the material viscoelastic properties. At high frequency, the effect of the material viscosity on the overall attenuation became more significant.

In chapter 5, a new ultrasonic testing technology for material characterization, Ultrasonic Dynamic mechanical analysis (U-DMA), has been applied to the viscoelasticity evaluation of particle reinforced polymer composites with different type and content of particles. Reasonable results of ultrasonic wave attenuation and viscoelastic characteristics are obtained by comparing with the result from time-domain finite element analysis for ultrasonic propagation in particulate composite materials. The multi-reflection and scattering waves due to particles, and the corresponding attenuation components, are emphasized and discussed with consideration of the mutual interactions among particles. By extracting and separately investigating the multi-reflection and

scattering waves, it is clear that the interactions among particles are playing a major role in the ultrasonic propagation and dynamic internal stress distribution. From the variation behavior of attenuation coefficient and viscoelasticity against particle weight fraction and incident wave frequency, the detailed influence mechanism of interactions among particles on both ultrasonic attenuation and viscoelastic characteristics are also clarified. Therefore, the newly developed Ultrasonic Dynamic Mechanical Analysis (U-DMA) method and the finite element analysis method for ultrasonic propagation in particulate composites are both proved to be reasonable and feasible in actual characterization of composite materials.

In conclusion, we can systematically and quantitatively evaluate the detailed correlation between material viscoelastic and anisotropy properties, ultrasonic propagation behavior and the internal stress distribution, interfacial and interparticle interactions and the incident ultrasonic wave characteristics, which will be useful for the further development of high-precision damage detection technology for composite material with various interfacial imperfections, and the results obtained from our study can provide strong guidance.

List of Publications

1. **Ran Li**, Toshiaki Natsuki, Qing-Qing Ni, A novel dynamic stress analysis in bimaterial composite with defect using ultrasonic wave propagation, **Composite Structures**, Volume 132 Pages: 255-264 Published: NOV 2015.
2. **Ran Li**, Qing-Qing Ni, Hong Xia, Toshiaki Natsuki, Analysis of Individual Attenuation Components of Ultrasonic Waves in Composite Material Considering Frequency Dependence, **Composites Part B: Engineering** (In press).
3. Qing-Qing Ni, **Ran Li**, Hong Xia, A new approach for Quantitative Evaluation of Ultrasonic Wave Attenuation in Composites, **Applied composite materials**, (In press).
4. **Ran Li**, Hong Xia, Qing-Qing Ni, Ya-Qin Fu, U-DMA measurement and dynamic analysis of ultrasonic wave propagation in particle reinforced composites. Composite science and technology (under review).

Scientific Presentation

- **International Conference**

1. **Ran Li**, Qing-Qing Ni, Yuma Arai, Hong Xia, Toshiaki Natsuki, Dynamic Stress Distribution of Composite Materials Using Ultrasonic Wave Propagation, The 11th China-Japan Joint Conference on Composite Materials (2014) ChongQing.
2. **Ran Li**, Toshiaki Natsuki, Qing-Qing Ni, A novel study of dynamic stress distribution using ultrasonic wave propagation analysis in bimaterial composite with defect, International Symposium on Fiber Science and Technology (2014) Tokyo.
3. **Ran Li**, Toshiaki Natsuki, Qing-Qing Ni, Quantitative analysis of ultrasonic scattering in particle reinforced composite materials, The 10th NANOSMAT International Conference on Surfaces, Coatings and Nanostructured materials (2015) Manchester.

- **Domestic Conference**

1. **Ran Li**, Toshiaki Natsuki, Qing-Qing Ni, Stress Concentration Phenomenon in Composite Materials Based on Ultrasonic Wave Propagation Simulation, The 5th Japan Conference on Composite Materials (2014) Kyoto.

2. **Ran Li**, Toshiaki Natsuki, Qing-Qing Ni, Analysis of ultrasonic wave attenuation in a composite model with a transverse elliptical defect, The 6th Japan Conference on Composite Materials (2015) Tokyo.

3. **Ran Li**, Toshiaki Natsuki, Qing-Qing Ni, Analysis of ultrasonic wave propagation in fiber reinforced composite materials with delamination and void, The 7th Japan Conference on Composite Materials (2016) Kyoto.

Acknowledgements

It is my great pleasure to express my gratitude to all those who gave me help and guidance during my PhD.

First of all, I want to give my sincere gratitude to my supervisor Prof. Qing-Qing Ni for supporting me, trusting me and encouraging me. Without Prof. Ni's help, I cannot complete my research.

I also want to express my grateful thanks to Prof. Toshiaki Natsuki for always giving me useful advises. In addition, I would like to thank to Prof. Hajime Konishi, Prof. Hiroaki Ishizawa, in Shinshu University, and Prof. Jing-long Wu in Okayama University for their advices and comments.

I want to express my gratitude to Interdisciplinary Graduate School of Science and Technology of Shinshu University, and Mitsubishi Corporation for the financial support.

Thanks to my friends in my laboratory: Li Zhang, Yao-Feng Zhu, Jing-Xing Shi, Xiao-Wen Lei, Yan Wang, Yu-Bing Dong, Melvin Gan Jet Hong, Takuo Hashizume, Ju-Hong Yu, Hai-Rong Chen, Jian Xing. Without yours help and support, the life in Japan will be very tough, and I cannot complete my PhD.

Finally, I want to thank my wife, thank you for always supporting me without any reservation.